Imperial College London
Department of Physics

MSc Quantum Fields and Fundamental Forces Project Report
The Effects of Short Pulse Duration and Aberrations on the Focus of a Laser

Michael Bloom
Imperial College London

September 2009

Supervised by Professor Roger Evans and Professor Kellogg Stelle

Abstract

The effects of short pulse duration and optical aberrations such as coma and astigmatism on the Electromagnetic fields present in the focus of a laser are investigated. Scalar diffraction theory is treated numerically to observe these effects and the results compared against experimental readings.

Contents

Acknowledgments

I would like to thank Professor Kellogg Stelle without who's support this project could never have been organized. Professor Roger Evans who gave up his time without any obligation to supervise this project and who has at all times been a source of leadership and sage advice. Dr Stuart Mangles for his help and advice, and for providing the experimental data for analysis. Nicolas-Pierre for his help and invaluable work arounds for both Fortran and Linux. Stefan Kneip for many useful matlab commands and Sabrina Nagel who has been my LATEXguru. I would also like to thank my parents for their love and support without which I would never have been able to complete this degree. Finally the very great number of people in both the Theory and Plasma physics groups of the Imperial college physics department who have at various time given up just a little of their day to help with a single line of code, ingenious work around, or equation.

1 Introduction

1.1 Statement of problem

In recent years it has become possible to shorten the duration of laser pulses to the extent that both femto-second and atto-second pulse durations can be reliably used to do experimental research [1]. This is of particular interest in Laser Wake Field Particle Acceleration [2], where, by focusing the peak power of the laser light to extreme intensities, the force exerted by these light pulses has been used to accelerate beams of electrons and protons to energies of a million volts over distances of only microns [3] [4].

These laser beams, which can consist of only a few wave lengths of radiation, constitute a problem for traditional Fraunhofer diffraction theory as the assumptions concerning the surfaces of integration can be invalid[1]. Specifically the focusing of these pulses has not yet been treated in a rigorous manner, and the effects of optical aberrations, such as coma, is unknown.

Thus a numerical treatment of diffraction theory, applicable to these short pulses, is attempted here and the effects of optical aberrations is examined. The results of this modelling are expanded to give a three dimensional map of the Electric and Magnetic fields about an optical focus; suitable as an input to Osiris or Epoch plasma codes. The numerical treatment is compared to experimental measurements made when an known optical aberrations are added to short laser pulses and measured near the focus. See Figures 2.1 and 4.1 (on pages 8 and 44).

1.2 Role of the Student

Three months is a short time to accomplish much in the way of serious research and although it is the opinion of the author that this report represents a some usefull progress, the author can not accept credit for it alone.

---

[1]See section for such short pulses(2.1.4) for discussion.

At the outset a working scalar diffraction code was already written, and it was the role of the student to build and develop that existing code. Indeed a great deal of time was spent becoming familiar with the Fortran 90 programing language, the MPI language-independent communications protocol[2], and the linux operating system. Further time was spent becoming familiar enough with diffraction theory to make any useful contribution to the existing code (even before any of the theoretical concerns of this report where addresed) and setting up a new workstation suitable for parallel processing, not to mention learning to use the LATEXtypesetting language (In which this report is written). However this was all accomplished, but not without the help of a great many people giving up valuable time from their day.

Then the student examined scalar diffraction theory and aberration theory in more depth deriving most of the important results and made appropriate changes in the code. Development of the numerical method by the student was mainly in the form of first verifying known results were reproduced correctly by the code. Secondly developing the code so that higher order aberrations could be included and so its out put compared with experiment. Thirdly developing a code which would give a idea of the kind of changes short pulse duration would cause in an image taken in the focal plane. This of course does not include the many blind alleys and mistakes along the way. The source codes included in this report do constitute an evolution from the original code but owe their construction to its form. Much time was spent using the new and current version of the codes to analyze the effects of short pulses (and checking that any new results were not the effect of numerical error).

Finally more work was done in researching a suitable vectorial theory which could be treated numerically in the same manner.

---

[2]Used to program parallel computers, and for this project to distribute the numerical burden over a number of computer processes.

2 Theory

2.1 Scalar Diffraction Theory

In order to study the focusing of short pulses of electromagnetic waves it is convenient to begin with a scalar theory. Thus such a theory will be formally examined. To motivate the discussion let us first discuss the model, so as the various aspects of diffraction theory are treated, their applicability to our modelling can be discussed.
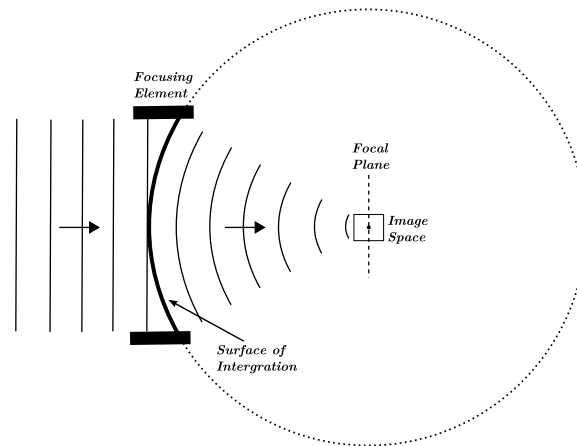
Figure 2.1: The setup of the spherical wave fronts, source plane and image space.

The focusing of short duration pulses of coherent laser light is to be modelled. The pulses are so short that they will, at most, consist of a few wave lengths of radiation. In experimental terms it is of interest to know the effects of optical aberrations on the electromagnetic fields near the focal point of focusing mirrors. It is convenient to model this as a spherical wave of varying amplitude passing through an aperture. See figure 2.1. In practise the parabolic mirrors are much larger in diameter than the laser pulse wave front. However this simply means that the aperture screen can

be thought of as having perfect conducting properties, so no amplitude of electromagnetic radiation passes, and the screen is infinitely narrow and so causes no edge effects. A perfect focusing mirror will in theory produce perfect spherical waves converging on the focal point of the mirror. This is of course never the case in practise. However the purpose of this modelling is to add aberrations to these ideal spherical waves. This may be accomplished by mathematical manipulation of the functions of these waves. Thus this is a reasonable modelling of the problem. So in our treatment of scalar diffraction theory let us start with Huygens' construction[5]:

> *Each point on a wavefront may be regarded as the center of a secondary disturbance which gives rise to spherical wavelets; The position of the wavefront at any later time is the envelope of all such wavelets.*

When combined with the principle of interference postulated by Fresnel[1] this yields what is know as the *Huygens-Fresnel Principle* and forms our basic model for the treatment of diffraction theory.

2.1.1 Scalar Diffraction Theory in Terms of Green's Functions

This principle was then taken by Kirchhoff [6] who showed that using Green's theorem an arbitrary point in the field P may be expressed in terms of the values of its solution and its first derivative on an arbitrary surface surrounding P. To demonstrate this consider an ideally monochromatic scalar wave

$$V(x, y, z, t) = U(x, y, z)e^{-i\omega t} \tag{2.1}$$

Note the time dependent part has been separated from the spatially dependent part U. Green's theorem gives

$$\int \int \int_v (U\nabla^2 f - f\nabla^2 U)dv = -\int \int_S \left(U\frac{\partial f}{\partial n} - f\frac{\partial U}{\partial n} \right) dS \tag{2.2}$$

Where $f(x, y, z)$ is an arbitrary function, and f and U are continuous in both first and second derivatives on and inside the surface S which encloses

---

[1]Superposed waves will constructively or destructively interfere according to their associated phase

a volume v, and n is the inward facing normal of S. Now U must satisfy the time-independent wave equation (Helmholtz equation) as it is a scalar wave, and let us consider the case where f also satisfies this equation

$$(\nabla^2 + k^2)U = 0 \qquad (2.3)$$

$$(\nabla^2 + k^2)f = 0 \qquad (2.4)$$

Where k is the wave number[2]. If $k \to 0$ these reduce to Laplace's equation $\nabla^2 U = 0$. So (2.3) and (2.4) inserted into (2.2) yields

$$\int \int_S \left(U \frac{\partial f}{\partial n} - f \frac{\partial U}{\partial n} \right) dS = 0 \qquad (2.5)$$

We have the freedom to choose the *Green's function* f as a single spherical wave expanding about P;

$$f(x, y, z) = \frac{e^{iks}}{s} \qquad (2.6)$$

where s is the distance from P. From (2.5) and (2.6) it is possible to arrive at the *integral theorem of Helmholtz and Kirchhoff* (To see full derivation see Appendix A on page 52):

$$U(P) = \frac{1}{4\pi} \int \int_S \left(U \frac{\partial}{\partial n} \left(\frac{e^{iks}}{s} \right) - \frac{e^{iks}}{s} \frac{\partial U}{\partial n} \right) dS \qquad (2.7)$$

As it happens most wave fronts may be considered as a sum of spherical waves, through the principle of superposition, and so this treatment is sufficient for our purpose. Obviously a monochromatic wave is an oversimplification but in the real laser systems that prompt this discussion the beams are very close to being band limited. This means the frequency spread of the waves can be included in the treatment of the pulse duration[3]. There does however exist a form of Kirchhoff Theorem for Non-Monochromatic Waves see [7].

Now let us consider the very simple case of diffraction through a aperture. This is useful for our calculations as the physical situation we will later model is a short pulsed laser beam being focused through a concave mirror

---

[2]$k = \omega/c$ where vacuum is assumed

[3]The convolution (multiplication in Fourier space) of an infinite monochromatic waveform with a finite pulse envelope yields a frequency band.

and this will be modelled as a spherical wave front (converging on our point of focus) passing through a aperture.

2.1.2 Kirchhoff's Boundary Conditions

For the purposes of this model let us consider the screen to be perfectly conducting so the electromagnetic field can be assumed to be zero inside it. Also let the screen be of a vanishingly small width, in comparison to the other lengths involved, so edge effects can be ignored. (This approach is most appropriate for a beam reflecting off a mirror where the beam diameter is less than that of the mirror).
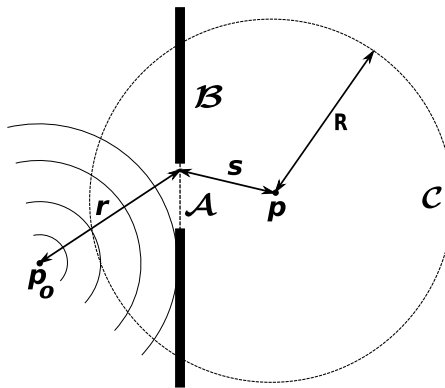
Figure 2.2: Integration surfaces

Consider the situation shown in Figure 2.2 where p_0 marks a source of spherical waves and p marks the point where the field is to be found. The surface of integration S can be spilt into three parts $\mathcal{A}, \mathcal{B}, \mathcal{C}$. Where $\mathcal{A}$ is the opening of the aperture. $\mathcal{B}$ is the surface of the screen and $\mathcal{C}$ is the arc of a sphere surrounding p of radius R. The *integral theorem of Helmholtz and Kirchhoff* (2.7) then becomes:

$$U(P) = \frac{1}{4\pi} \left\{ \int\int_{\mathcal{A}} + \int\int_{\mathcal{B}} + \int\int_{\mathcal{C}} \right\} \left(U \frac{\partial}{\partial n} \left(\frac{e^{iks}}{s} \right) - \frac{e^{iks}}{s} \frac{\partial U}{\partial n} \right) dS \quad (2.8)$$

What is known as the as the *Kirchhoff boundary conditions* [7] can now be

applied to the boundaries $\mathcal{A}$ and $\mathcal{B}$:

$$\mathcal{A}: \quad U = U_{in}, \quad \frac{\partial U}{\partial n} = \frac{\partial U_{in}}{\partial n} \qquad (2.9)$$

$$\mathcal{B}: \quad U = 0, \quad \frac{\partial U}{\partial n} = 0 \qquad (2.10)$$

Where U_{in} is the field due to the point p_0 . So across the surface $\mathcal{A}$ the field is assumed to be the same as if the aperture is not present. This assumption is not always acceptable for the treatment of the field very near to the aperture. However as already mentioned, in our case we model a wave front which is of finite diameter being focused by a large parabolic mirror. We are only interested in the field near focus. So this assumption is valid, as is the assumption that the fields over surface $\mathcal{B}$ are zero. For the surface $\mathcal{C}$ we are free to make the radius R arbitrarily large. If we wish to know the field at a time t and we let $R \gg ct$ the field due a p_0 may be considered to be zero, as causally the points will not be connected. These conditions yield what is know as the *Fresnel-Kirchhoff diffraction formula*:

$$U(P) = -\frac{iA}{2\lambda} \int_{\mathcal{A}} \frac{e^{ik(r+s)}}{rs} \left[cos(n,r) - cos(n,s) \right] dS \qquad (2.11)$$

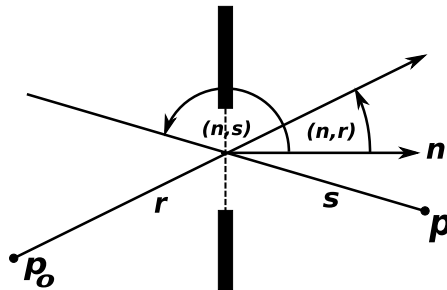where the angles are defined as in Figure 2.3.

Figure 2.3: Angles

Though this treatment gives in practise the correct experimental results there is, however, a problem. As it can be shown that for the Helmholtz equation (2.3) that if $U = 0$ and $\frac{\partial U}{\partial n} = 0$ over any finite surface, then $U = 0$ everywhere [8].

2.1.3 Rayleigh Boundary Conditions

A resolution to the problem posed by the Kirchhoff approximation is attributed to Rayleigh [8]. The problem can be resolved with the selection of an appropriate Green's function satisfying both the Dirichlet[4] and Neumann[5] boundary conditions. The Dirichlet Green's function is then:

$$U_D(\mathbf{x}, \mathbf{x'}) = 0 \tag{2.12}$$

Where $\mathbf{x}$ is the position vector of the point of interest P and $\mathbf{x'}$ is the position vector on the boundary surface. This yields, in the same manner as (2.11), the generalised Kirchhoff integral:

$$U(\mathbf{x}) = \int_S U(\mathbf{x'}) \frac{\partial U_D}{\partial n'}(\mathbf{x}, \mathbf{x'}) da' \tag{2.13}$$

The Neumann Green's function is then:

$$\frac{\partial U_N}{\partial n'}(\mathbf{x}, \mathbf{x'}) = 0 \tag{2.14}$$

and this yields the generalised Kirchhoff integral:

$$U(\mathbf{x}) = -\int_S \frac{\partial U}{\partial n'}(\mathbf{x'}) U_N(\mathbf{x}, \mathbf{x'}) da' \tag{2.15}$$

For (2.12) a consistent approximation is that the Green's function is zero everywhere but the openings, and the same as the incident wave at the openings. A similarly consistent approximation can be formulated for (2.14). However they can not be taken together without running into the Kirchhoff Boundary Problem. If both P_0 and P are taken to be many wavelengths away from the screen the fields for the three approximations (Dirichlet, Neumann, and Kirchhoff) can be written in the common form [8]:

$$U(P) = \frac{k}{2\pi i} \int_{\mathcal{A}} \frac{e^{ik(r+s)}}{rs} \Theta(\theta, \theta') dS \tag{2.16}$$

---

[4]A boundary condition of the first type; When imposed on a differential equation, specifies the values a solution takes on the boundary of the domain.

[5]A boundary condition of the second type; when imposed of a differential equation, specifies the values the derivative of solution takes on the boundary of the domain.

where

$$\Theta(\theta, \theta') = \begin{cases} cos\theta & \text{Dirichlet Approximation} \\ cos\theta' & \text{Neumann Approximation} \\ \frac{1}{2}(cos\theta + cos\theta') & \text{Kirchhoff Approximation.} \end{cases}$$

$\Theta(\theta, \theta')$ is known as the *obliquity factor* (or sometimes *inclination factor*), where θ and θ' are the angles (n, r) and (n, s) respectively. From this it is apparent why Kirchhoff's approximations, though mathematically inconsistent, could give results which to a high degree of accuracy appear to be correct. For when P and P_0 are far from the screen the obliquity factor is essentially constant, for the areas of the diffraction pattern which have appreciable intensity, for the different approximation schemes. This yields the same relative intensities in the diffraction pattern. Further, for normal incidence, the obliquity factors are all approaching unity.

The differences shown by these approximation schemes is a sign that we are reaching the limits of what a scalar theory of diffraction can tell us. To resolve these problems it is necessary to form a more elaborate physical theory and move to a vector theory of diffraction, as these fields are, of course, really vector fields. For the purposes of the computational model which is being constructed, it is not necessary to include the obliquity factor. In the geometry that is used the angles are around 10^{-3} radians and the cosine is unity to within 1 part in 10^6.

2.1.4 Fraunhofer and Fresnel Diffraction

A discussion of scalar diffraction theory would be remiss if mention was not made of Fraunhofer and Fresnel approximations. Consider the kernel of (2.15), and let us rewrite it as:

$$U(x_0, y_0) = \int_x \int_y h(x_0, y_0; x, y)U_s(x, y)dxdy \qquad (2.17)$$

where U_S is the source field at the screen, x_0 and y_0 are the coordinates of point P and x and y the coordinates on the surface $\mathcal{A}$ and the kernel:

$$h(x_0, y_0; x, y) = \frac{i}{\lambda}\Theta(\theta, \theta')\frac{e^{iks}}{s} \qquad (2.18)$$

14

When the diameter of the aperture is much smaller than the distance to the focal plane (or the point p), the $\frac{1}{s}$ term can be approximated as $\frac{1}{f_0}$ where f_0 is the distance of P from $\mathcal{A}$. Which leaves the e^{iks} term which can not be approximated in this way as the s multiplied by the 'large' k number. As

$$s = \sqrt{z_0^2 + (x - x_0)^2 + (y - y_0)^2} \tag{2.19}$$

taking the Taylor expansion

$$s \cong z_0 \left(1 + \frac{1}{2} \left(\frac{x - x_0}{z_0} \right)^2 + \frac{1}{2} \left(\frac{y - y_0}{z_0} \right)^2 + ... \right) \tag{2.20}$$

$$= z_0 \left(1 + \frac{x_0^2 + y_0^2}{2z_0^2} - \frac{xx_0 + yy_0}{z_0^2} + \frac{x^2 + y^2}{2z_0^2} + ... \right) \tag{2.21}$$

The *Fresnel approximation* truncates the series after the first term so

$$h(x_0, y_0; x, y) \cong \frac{i}{\lambda} \Theta(\theta, \theta') \frac{e^{ikz_0}}{z_0} e^{i\frac{k}{2z_0}((x-x_0)^2 + (y-y_0)^2)} \tag{2.22}$$

[7] This yields what is know as Fresnel's integral in equation (2.17) and lacks analytic solutions due to the square dependence on the integration variable.

The *Fraunhofer approximation* truncates the series to neglect the square dependence on the integration variable completely

$$h(x_0, y_0; x, y) \cong \frac{i}{\lambda} \Theta(\theta, \theta') \frac{e^{ikz_0}}{z_0} e^{i\frac{k}{2z_0^2}(x_0^2 + y_0^2)} e^{i\frac{k}{z_0^2}(xx_0 + yy_0)} \tag{2.23}$$

As for the purposes of the integration x_0, y_0 are constants. This is equivalent in (2.17) to a two dimensional Fourier transform.

The numerical treatment outlined in this report differs from these common treatments by evaluating the value of s from (2.19) to high numerical precision, and so, is in many ways more accurate than the Fraunhofer and Fresnel approximations. The necessity of doing this is due to the function U_s really being dependent on s due to the effect of having a short pulse envelope.

2.2 Transformation to E and B Fields from Scalar Diffraction Theory

The intensity of the electromagnetic field is defined as the magnitude of the Poynting vector and given by

$$I = \frac{c}{4\pi} | < \vec{E} \times \vec{H} > |$$ (2.24)

So naively the intensity given in terms of our scalar field U by

$$I \propto |U|^2$$ (2.25)

and this is used throughout the numerical analysis here. However there are times when one wishes to retrieve the electric and magnetic field vectors (for instance for use in the Osiris or Epoch particle in cell code). Through considering the field due to a monochromatic point dipole oscillator it can be shown [7] that

$$\vec{E}(x_i, y_i, z_i, t) = \Re\left\{\frac{\omega^2}{c^2} U(x_i, y_i, z_i)\vec{\alpha}e^{-i\omega t}\right\}$$ (2.26)

and

$$\vec{H}(x_i, y_i, z_i, t) = \Re\left\{\frac{\omega^2}{c^2} U(x_i, y_i, z_i)\vec{\beta}e^{-i\omega t}\right\}$$ (2.27)

where $\vec{\alpha}$ and $\vec{\beta}$ are normal unit vectors in the plane perpendicular to x_3 and x_3 is defined in Figure 2.4.
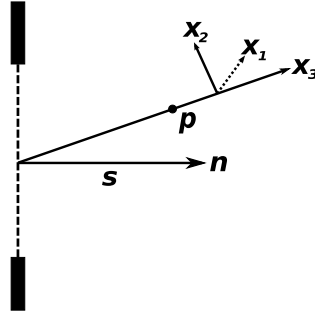
Figure 2.4: The coordinates of the space in which $\vec{\alpha}$ and $\vec{\beta}$ are defined.

If we are dealing with incoming polarised radiation it is possible to work

out the field vectors using these formulae and simple geometric considerations. In fact it has been done in [9]. However verification that the Maxwell's laws are upheld in the resulting fields in the direction of focus is necessary. This is a topic for future work.

2.3 Theory of Aberrations

In this section an overview of aberration theory will be given. Presenting first the geometrically derived Seidel Aberrations and then moving to the more expansive treatment through what are known as the Zernike Polynomials.

2.3.1 Seidel Aberrations

Some of the most important investigations in this field can be attributed to Schwarzschild [10]. Schwarzschild used a method similar to that which he used in his calculations of orbital elements in celestial mechanics[6]. He introduces variables which, in the accuracy of Gaussian optics, have constant values along each ray passing though the optical system. With the help of a perturbation function which he called the *Seidel eikonal* he found the changes to the variables due to fourth order terms in the expansion of the perturbation function. The variables he named *Seidel Variables* after the variables used by Seidel in his earlier work [11].

The derivation is too involved to be included here but it can be shown that the Seidel variables restrict the aberrations to changes of the phase of the form

$$\delta = \chi \rho^m (\cos \theta)^n \tag{2.28}$$

where χ is a constant and m and n are positive real integers. However for δ to be single valued

$$\rho \to -\rho \text{ and } \theta \to \theta + \pi$$

must leave δ unchanged. Thus the value of $(m + n)$ is restricted to being even. A further restriction is that $n \leqslant m$, to be well behaved near the origin.

Thus the perturbation eikonal of Schwarzschild takes the form [7]

$$\phi = -\frac{1}{4}B\rho^4 - Cy_0^2\rho^2\cos^2\theta - \frac{1}{2}Dy_0^2\rho^2 + Ey_0^3\rho\cos\theta + Fy_0\rho^3\cos\theta... \tag{2.29}$$

where $\xi = \rho \sin \theta$ and $\eta = \rho \cos \theta$ are Cartesian and polar coordinates in the source plane. The aberration components on the wave fronts are in this

---

[6]In his method treating celestial mechanics variables are introduced which remain constant in the unperturbed motion. The small changes which these quantities actually undergo in actual motion are then determined with the help of a perturbation function.

form

$$\Delta x = B\rho^3 \sin\theta - 2Fy_0\rho^2 \sin\theta\cos\theta + Dy_0^2\rho\sin\theta \qquad (2.30)$$

$$\Delta y = B\rho^3 \cos\theta - 2Fy_0\rho^2(1 + 2\cos^2\theta) + (2C + D)y_0^2\rho\cos\theta - Ey_0^3 \quad (2.31)$$

The aberrations due to each of the coefficients not being zero have associated names:

- $m = 0, n = 0$ means $\delta =$ constant this is just a translation of the lens and referred to as *Piston*.

- If $m = 1$ then $n = 1$. $\delta = \chi\rho\cos\theta$. So $E \neq 0$ and this is called *Distortion* or sometimes a type of *Tilt*.

- $m = 2, n = 0$ means $\delta = \chi\rho^2$ so $D \neq 0$ which changes the focal length of the lens and is sometimes called *shift of focus* or *Curvature of field*.

- $m = 2, n = 2$ means $\delta = \chi\rho^2(\cos\theta)^2$ so $C \neq 0$ and this is known as *Astigmatism*[7].

- $m = 3, n = 1$ means $\delta = \chi\rho^3\cos\theta$ so $F \neq 0$ and this is called *Coma*. As the coma introduces a net tilt into the beam in the Seidel formalism a $\rho\cos\theta$ term is used to cancel the tilt. So $\delta = \chi\left(\rho^4 - \rho\right)\cos\theta$.

- $m = 4, n = 0$ means $\delta = \chi\rho^4$ so $B \neq 0$ and corresponds to what is known as *Spherical aberration*. This also causes an axial shift of focus so again commonly in the Seidel formalism this is canceled with a ρ^2 term. So $\delta = \chi(\rho^4 - \rho^2)$.

There are of course higher order aberrations but they are rarely named. The effects on the wavefront of some of these aberrations are shown in Figure 2.5.

2.3.2 Zernike Polynomials

For the purpose of convenience, the aberration function ϕ can be expanded in terms of a *complete set* of polynomials which are orthogonal over the interior of the unit circle. Though there are many sets of polynomials which

---

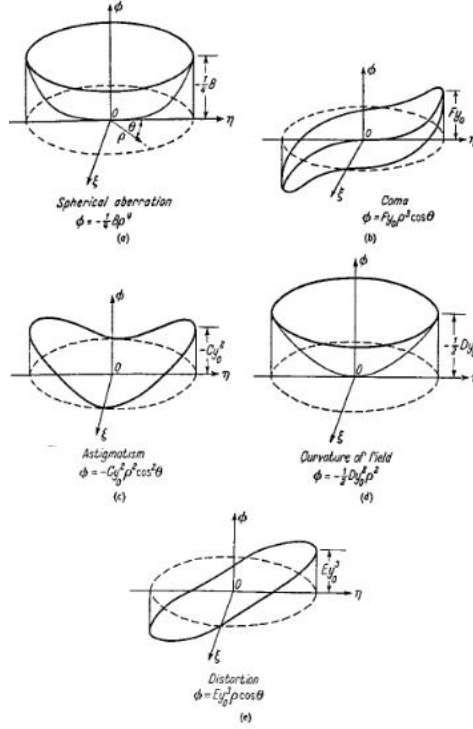[7]Note the form of Astigmatism changes slightly in the Zernike formulation

Figure 2.5: The primary wave aberations. (*reproduced from Born and Wolf Principles of Optics* [7].)

are complete and fulfil this property, one set known as the Zernike polynomials is of particular interest as it has certain invariance properties. The Zernike polynomials are of the form

$$V_n^l(\rho \sin \theta, \rho \cos \theta) = R_n^l(\rho) e^{il\theta}$$

where $\rho \sin \theta = X$ and $\rho \cos \theta = Y$ where X and Y are real. The radial polynomials are given by

$$R_n^{\pm m}(\rho) = \sum_{s=0}^{\frac{n-m}{2}} (-1)^s \frac{(n-s)!}{s! \left(\frac{n+m}{2} - s\right)! \left(\frac{n-m}{2} - s\right)!} \rho^{n-2s}$$

Where $m = |l|$

In section 4 an adaptive optics system is utilised which uses the Zernike polynomials in a particular form. This form is shown in Figure 2.6.

#	Name	PrV/RMS Factor	Cartesian form (RMS)	n (radial)	m (azimuthal)	Polar Form (RMS)
1	Piston	1	1	0	0	1
2	Tilt X	2	$\sqrt{4}\,x$	1	1	$\sqrt{4}\,\rho\cos(\theta)$
3	Tilt Y	2	$\sqrt{4}\,y$	1	-1	$\sqrt{4}\,\rho\sin(\theta)$
4	Defocus	$\sqrt{3}$	$\sqrt{3}(2x^2+2y^2-1)$	2	0	$\sqrt{3}(2\rho^2-1)$
5	0° Astigmatism	$\sqrt{6}$	$\sqrt{6}(x^2-y^2)$	2	2	$\sqrt{6}\rho^2\cos(2\theta)$
6	45° Astigmatism	$\sqrt{6}$	$\sqrt{6}(2xy)$	2	-2	$\sqrt{6}\rho^2\sin(2\theta)$
7	Coma X	$\sqrt{8}$	$\sqrt{8}(3x^3+3xy^2-2x)$	3	1	$\sqrt{8}(3\rho^3-2\rho)\cos(\theta)$
8	Coma Y	$\sqrt{8}$	$\sqrt{8}(3x^2y+y^3-2y)$	3	-1	$\sqrt{8}(3\rho^3-2\rho)\sin(\theta)$
9	30° Trefoil	$\sqrt{8}$	$\sqrt{8}(x^3-3xy^2)$	3	3	$\sqrt{8}\rho^3\cos(3\theta)$
10	0° Trefoil	$\sqrt{8}$	$\sqrt{8}(3x^2y-y^3)$	3	-3	$\sqrt{8}\rho^3\sin(3\theta)$
11	Spherical Aberration	$\sqrt{5}$	$\sqrt{5}(6x^4+12x^2y^2+6y^4-6x^2-6y^2+1)$	4	0	$\sqrt{5}(6\rho^4-6\rho^2+1)$
12	0° Secondary Astigmatism	$\sqrt{10}$	$\sqrt{10}(4x^4-3x^2+3y^2-4y^4)$	4	2	$\sqrt{10}(4\rho^4-3\rho^2)\cos(2\theta)$
13	45° Secondary Astigmatism	$\sqrt{10}$	$\sqrt{10}(8x^3y+8xy^3-6xy)$	4	-2	$\sqrt{10}(4\rho^4-3\rho^2)\sin(2\theta)$
14	0° Tetrafoil	$\sqrt{10}$	$\sqrt{10}(x^4-6x^2y^2+4y^4)$	4	4	$\sqrt{10}\rho^4\cos(4\theta)$
15	22.5° Tetrafoil	$\sqrt{10}$	$\sqrt{10}(4x^3y-4xy^3)$	4	-4	$\sqrt{10}\rho^4\sin(4\theta)$
16	Secondary X Coma	$\sqrt{12}$	$\sqrt{12}(10x^5+20x^3y^2+10xy^4-12x^3-12xy^2+3x)$	5	1	$\sqrt{12}(10\rho^5-12\rho^3+3\rho)\cos(\theta)$
17	Secondary Y Coma	$\sqrt{12}$	$\sqrt{12}(10x^4y+20x^2y^3+10y^5-12x^2y-12y^3+3y)$	5	-1	$\sqrt{12}(10\rho^5-12\rho^3+3\rho)\sin(\theta)$
18	Secondary 0° Trefoil	$\sqrt{12}$	$\sqrt{12}(5x^5-10x^3y^2-15xy^4-4x^3+12xy^2)$	5	3	$\sqrt{12}(5\rho^5-4\rho^3)\cos(3\theta)$
19	Secondary 30° Trefoil	$\sqrt{12}$	$\sqrt{12}(15x^4y+10x^2y^3-5y^5-12x^2y+4y^3)$	5	-3	$\sqrt{12}(5\rho^5-4\rho^3)\sin(3\theta)$
20	18° Pentafoil	$\sqrt{12}$	$\sqrt{12}(x^5-10x^3y^2+5xy^4)$	5	5	$\sqrt{12}\rho^5\cos(5\theta)$
21	0° Pentafoil	$\sqrt{12}$	$\sqrt{12}(5x^4y-10x^2y^3+y^5)$	5	-5	$\sqrt{12}\rho^5\sin(5\theta)$

Figure 2.6: The Zernike Polynomials as used in the adaptive optics system[12].

2.4 Vector Diffraction Theory

Both the Fresnel-Kirchhoff and Rayleigh-Sommerfeld formulations of the scalar theory of diffraction are well used and verified theories [7] [13] [14]. Indeed most formulations of scalar diffraction theory use the integral theorem of Kirchhoff outlined in Section 2.1. However the electromagnetic fields are by their nature vectorial. So it is inevitable that in some applications is it is necessary to have a vector theory of diffraction[8].

Attempts have been made to do this from regaining the field vectors from the scalar theory. For instance through the Rayleigh-Sommerfeld theory in used in [15] [16] and regaining the field vectors was considered in Section 2.2.

What is known as the Richards-Wolf formulation [17] represents a vec-

---

[8]For instance when the polarisation is not uniform over the input aperture or for optics with very low f-number.

tor diffraction theory where a vectorial equivalent of the Fresnel-Kirchoff diffraction integral known as the Stratton-Chu integral [18] has been used along with the Kirchhoff boundary conditions to create a vector theory. This is in fact used in [9] to look at the effects of short pulses being focused, though aberrations are not considered whereas here they are.

The Richards-Wolf formalism is further developed and used in [19]. Into what is known as Hertz Vector Diffraction Theory (HVDT), which is closely related to the vector potential commonly used in electromagnetism. This theory is of particular interest if one is to do further numerical work using the electromagnetic field vectors as it assures that the resulting diffraction pattern satisfies all the Maxwell equations. This is of particular use for use with plasma codes such as Osiris or Epoch. For if the equations are not satisfied in the input to such codes, they will still represent a valid superposition of fields. This leads to startup artifacts (extra erroneous electromagnetic waves), in the simulations.

However other formulations of Vector Diffraction Theories for electromagnetic waves exist, for instance the vector Huygens-Fresnel theory developed in [20] which use the field equivalence theorems, outlined in [21] and [22].

2.4.1 Richards-Wolf formulation

The Richards-Wolf formulation (given in [17]) for a lens uniformly illuminated by a polarised beam is

$$\vec{E} = E_x(P)\vec{e_x} + E_y(P)\vec{e_y} + E_z(P)\vec{e_z} \tag{2.32}$$

where $P(x_i, y_i, z_i)$ is the point of observation in the image plane. $\vec{e_x}$, $\vec{e_y}$, and $\vec{e_z}$ are unit vectors orthogonal to each other and along the coordinate axis of the optical system (x, y, z).

In terms of the optical coordinates [9], $u = (k\sin^2\alpha)z$ and $v = (k\sin\alpha)r$ where $k = n2\pi/\lambda$ and $r = (x_i^2 + y_i^2)^{1/2}$. n is the refractive index of the medium and α is the angular semi-aperture on the image side, $0 \leqslant \alpha \leqslant \pi/2$. The elements of $\vec{E}$ are given by:

$$E_x(P) = -i(I_0 + 2I_2\cos\phi) \tag{2.33}$$

$$E_y(P) = -iI_2\sin\phi \tag{2.34}$$

22

$$E_x(P) = -2I_1 \cos \phi \tag{2.35}$$

and

$$I_0(u,v) = \int_0^\alpha \cos^{1/2} \theta \sin \theta (1 + \cos \theta) J_0 \frac{v \sin \theta}{\sin \alpha} \exp \left(\frac{iu \cos \theta}{\sin^2 \alpha} \right) d\theta \tag{2.36}$$

$$I_1(u,v) = \int_0^\alpha \cos^{1/2} \theta \sin^2 \theta J_1 \frac{v \sin \theta}{\sin \alpha} \exp \left(\frac{iu \cos \theta}{\sin^2 \alpha} \right) d\theta \tag{2.37}$$

$$I_2(u,v) = \int_0^\alpha \cos^{1/2} \theta \sin \theta (1 - \cos \theta) J_2 \frac{v \sin \theta}{\sin \alpha} \exp \left(\frac{iu \cos \theta}{\sin^2 \alpha} \right) d\theta \tag{2.38}$$

Where J_m is the Bessel function defined in Equation 3.11, ϕ is the azimuth angle giving the polarization direction of the field.

3 Numerical Treatment

3.1 Numerical Treatment of Scalar Theroy

3.1.1 Aim

The aims of the numerical treatment were to produce a code that would accurately produce values for the scalar field, within the limits of validity of the scalar theory, near to the focus of a focusing parabola, for laser beams contained within envelope functions of duration equal to a few laser wavelengths. Further the code must be able to apply primary optical aberration to the incoming wave front. This was accomplished and an example of the source code is presented in appendix B.1.

The next aim was to compare output of the code with real experimental laser pulses. For this is was necessary to make another code to vary the field over time, carry out a time integration, and produce an image of what a detector might see. This was accomplished and an example of the source code is presented in appendix B.2.

The code must also allow for further work on the numerical treatment of scalar diffraction theory, such as: creating values of the separate electric and magnetic field vectors, from the scalar field theory, with sufficient resolution to be used in existing plasma particle in cell codes.

3.1.2 Methodology

From Section 2.1 we are left with the generalized Kirchhoff-Fresnel-Rayleigh diffraction formula of the form:

$$U(P) = -\frac{iA}{2\lambda} \int_{\mathcal{A}} \frac{e^{ik(r+s)}}{rs} \Theta(\theta, \theta') dS \qquad (3.1)$$

Which may be rewritten for an arbitrary incoming wavefront as:

$$U(P) = -\frac{i}{2\lambda} \int \int_{\mathcal{A}} U_{in}(x_s, y_s) \frac{e^{iks}}{s} \Theta(\theta, \theta') dx_s dy_s \qquad (3.2)$$

Where $U_{in}(x_s, y_s)$ represents the amplitude of the incoming field over the integration surface $\mathcal{A}$ and $\Theta(\theta, \theta')$ is the inclination factor. The distance s of point $P(x_i, y_i)$ to a point on $\mathcal{A}$ is of course a function of the following variables $s(x_s, y_s; x_i, y_i)$.

To obtain a 3D distribution of the scalar field is just a case of numerically integrating equation (3.2). This may be accomplished through the use of a few nested loops. Though this, depending on the accuracy required, can be very computationally intensive it lends itself well to parallel processing. Which leads to the basic form of the two source codes developed listed in appendix B.1 and B.2.

The inclination factor was approximated as unity and discarded for the reasons set forward on page 14; it simply is not large enough to be numerically relevant. At least not in the systems that are considered here. However if low f-number systems are considered it will become important[1]. It is dependant on the cosine of angle between the normal of the integration surface and the point of interest. When this becomes significant it may be included in the code relatively simply.

The surface of integration was chosen to be a spherical section of radius equal to the (non aberrated) focal length of the mirror. This has the advantage of corresponding to a surface of constant phase for a perfectly focused beam[2]. The code produces the integration surface as an array of points each with its own spatial coordinate and the aberrations from Section 2.3 are then added as changes to the phase of the wavefront across this surface. Care must be taken to insure that the number of points comprising the surface of integration (the source plane) is large enough

A) To capture the fine details of any aberration functions added.

B) So as not to produce numerical artifacts in the image plane due to the surface of integration being coarse when mathematically it should be smooth.

Obviously any increase in the number of points in the integration surface

---

[1] In systems of f-number less than ≈ 3 the inclination factor may become important.

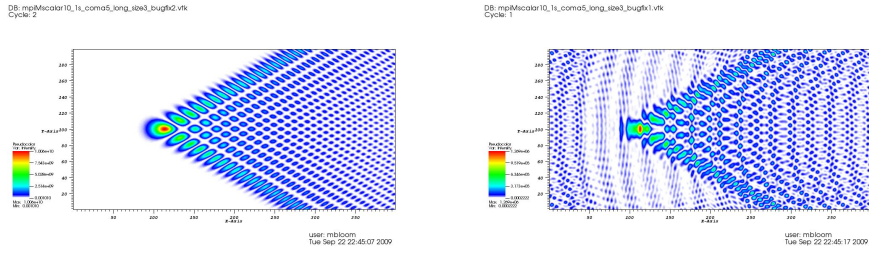[2] That is to say, a beam which will converge on a single point.

Figure 3.1: This is the magnitude of the scalar electromagnetic field in the image plane due to a continuous incident wave with an aberration of 5 wavelengths of coma in the x direction. Each step on the axis represents 1μm in real space, with the unaberrated focus located at point (300,100). The figure on the left has a source plane of 4000x4000 data points. The figure on the right 400x400. There is no other difference in the calculation which produced the images.

will drastically increase computational burden so a compromise must be made as always. In practise there is a minimum number of surface points for which any further increase will not cause any, physically significant, change in the calculated values in the image space. However this minimum number is dependent on not only the density of points in the image space one wishes to produce values for, but also on the nature of the incoming wavefront, and its variation in amplitude and phase (associated with any aberrations). So in practise the minimum density of points in the source plane can not be known for a general case and must be found depending on the application the code is to be put to. Figure 3.1 demonstrates this kind of error. As one can see there is a periodic distortion caused by having too few points in the source plane. Figure 3.2 shows that no further change to the image occurs after the number of points in the source plane is increased from 1600 by 1600 to 4000 by 4000[3].

Once the integration surface is produced the code splits the image space into multiple parts for parallel processing. For each point in the image space the contribution from each point in the source plane is calculated with its appropriate phase and added to the real or imaginary total of the field as befits its phase. In this 'brute force' manner the numerical integration is carried out. It is also during this stage that the variation of amplitude due to

---

[3]Unfortunately a run with 4000x4000 data points in the source plane and 200x400 in the image plane takes about two and a half days to run on 8 cpu's.
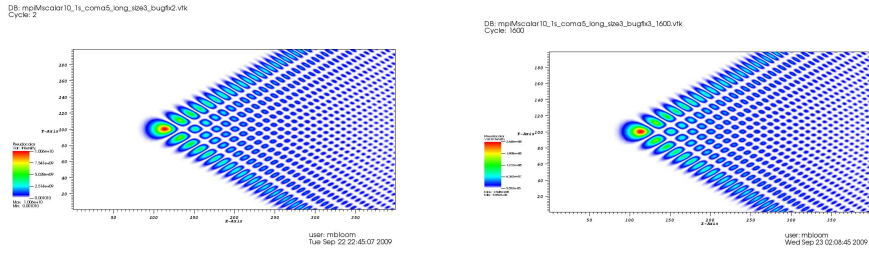
26

Figure 3.2: This is the magnitude of the scalar electromagnetic field in the image plane due to a continuous incident wave with an aberration of 5 wavelengths of coma in the x direction. Each step on the axis represents 1μm in real space, with the unaberrated focus located at point (300,100). The figure on the left has a source plane of 4000x4000 data points. The figure on the right 1600x1600. There is no other difference in the calculation which produced the images.

finite pulse duration is included though an envelope function. This is done by changing the amplitude of each point in the source plane depending on its distance to the point in the image plane and the distance to the center of focus. For the purposes of this analysis the amplitude of the pulse should be varied by a function which goes smoothly to zero. With that in mind the following function was used:

$$f(t) = \begin{cases} t^4 - 2t^2 + 1 & \text{when} -1 \leq t \leq 1 \\ 0 & \text{otherwise.} \end{cases} \tag{3.3}$$

The amplitude of the points on the source plane is then varied using $f(t)$ while making t a function of phase, which has the values -1 and +1 at some number of wavelengths from the pulse maximum. In future work the pulse amplitude may be varied from data on real laser pulses here instead.

Essentially the calculation becomes the sum:

$$U(P) = -\frac{i}{2\lambda} \sum_{x_s} \sum_{y_s} A(\phi, A_{in}) \frac{e^{i\phi(x_s, y_s, s)}}{s} \Delta x_s \Delta y_s$$

Where the function A depends on the amplitude of the scalar field at the point (x_s, y_s) on source plane and the envelope function.

3.1.3 Time integrated Scalar Code

If the calculated values of the electromagnetic field are to be compared to experimental results one must consider what would be recorded by a measuring device. A device such as a CCD camera would take an image related to the energy of the electromagnetic wave incident on each of its pixels over a finite period time.

The amount of energy present in an electromagnetic wave is related to the Poynting vector $\mathbf{S}$ which represents the amount of energy which crosses per second a unit area normal to the $\mathbf{E}$ and $\mathbf{B}$ fields.

$$\mathbf{S} = \frac{c}{4\pi}(\mathbf{E} \times \mathbf{B}) \tag{3.4}$$

where

$$\frac{\partial u}{\partial t} + \nabla \cdot \mathbf{S} = -\mathbf{J} \cdot \mathbf{E} \tag{3.5}$$

As this interpolation of the Poynting vector involves only the divergence of $\mathbf{S}$ it may not be unique as any curl of any vector may be added without changing its divergence[4]. However as discussed in [8] relativistic considerations show that $\mathbf{S}$ is unique.

If as $\mathbf{E}$ and $\mathbf{B}$ are assumed to be perpendicular and related to our scalar field $U(\mathbf{s})$ as described above then

$$\mathcal{E} = \int_{\mathrm{A}} \mathbf{S} d\mathbf{A} \propto \left(\Re\left\{U(\mathbf{s})\right\}\right)^2 + \left(\Im\left\{U(\mathbf{s})\right\}\right)^2 \tag{3.6}$$

where the integral is over the area A and $\mathcal{E}$ gives a measure of the energy flux thorough A. So to get a measure of the energy deposited by a laser beam one is intrested in the time integrated value

$$\int_a^b \mathcal{E} dt$$

For a continuous beam laser $|\mathbf{S}|$ may not vary appreciably in time. However for our purposes we will assume the pulse duration of our envelope function is smaller than the time resolution of what ever measuring device we are

---

[4]As $\nabla \cdot (\nabla \times \mathbf{a}) = 0$

considering. Thus

$$\sum_t \mathcal{E}\Delta t \propto \sum_t \left([\Re\{U(\mathbf{x}, t)\}]^2 + [\Im\{U(\mathbf{x}, t)\}]^2 \right) \Delta t$$

is a quantity which should be proportional to the readings from a measuring device such as a CCD. For that reason the code in Appendix B.2 was written to calculate the field at the focal plane of the focusing device at different time steps and then add them to give an image suitable for comparison with experimental results.

3.2 Verification of the Scalar Code though Known Results

In order to verify whether the numerical treatment of the scalar theory which was developed in fact gives physically meaningfull results, its output may be compared to known analytical solutions.

3.2.1 Airy Pattern

One of the best known analytical solutions is the so called *Airy Ring Pattern* which occurs when a wave front of constant amplitude is incident on a circular diffracting aperture[5]. For the treatment on page 15 and equations (2.17) and (2.23) we have in terms of the Fraunhofer approximation:

$$U(x_0, y_0) = \int_{x_s} \int_{y_s} \frac{i}{\lambda} \Theta(\theta, \theta') \frac{e^{ikz_0}}{z_0} e^{i\frac{k}{2z_0^2}(x_0^2 + y_0^2)} e^{i\frac{k}{z_0^2}(x_s x_0 + y_s y_0)} U_s(x_s, y_s) dx_s dy_s \tag{3.7}$$

Assuming a flat top beam and neglecting the inclination factor this becomes

$$U(x_0, y_0) = C \int_{x_s} \int_{y_s} e^{-ik(x_s x_0 + y_s y_0)} dx_s dy_s \tag{3.8}$$

where C is a constant that includes the (constant function) $U_s(x_s, y_s)$ and all the other constant terms. Making a change of variables

$$\rho\cos\theta = x_s \quad \rho\sin\theta = y_s$$
$$w\cos\psi = x_0 \quad w\sin\psi = y_0$$

---

[5]This is sometimes called a flat top beam profile.

So[6],

$$U(x_0, y_0) = C \int_0^a \int_0^{2\pi} e^{-ik\rho w \cos(\theta - \psi)} \rho d\rho d\theta \tag{3.9}$$

Thus

$$U(x_0, y_0) = 2\pi C \int_0^a J_0(k\rho w) \rho d\rho \tag{3.10}$$

where J_0 is a Bessel function of the general form:

$$J_n = \frac{i_{-n}}{2\pi} \int_0^{2\pi} e^{ix\cos\alpha} e^{in\alpha} d\alpha \tag{3.11}$$

with recurrence relation:

$$\frac{d}{dx} \left[x^{n+1} J_{n+1}(x) \right] = x^{n+1} J_n(x)$$
$$\int_0^x x' J_0(x') dx' = x J_1(x)$$

So

$$U(x_0, y_0) = a^2 \pi C \left[\frac{2 J_1(kaw)}{kaw} \right] \tag{3.12}$$

and the intensity is

$$I(x_0, y_0) = |U(x_0, y_0)|^2 = I_0 \left[\frac{2 J_1(kaw)}{kaw} \right]^2 \tag{3.13}$$

Figure 3.3 shows predicted intensity for a continuous beam. As one can see the agreement is good. This shows that the code at least agrees with established theory over this well known result.

3.2.2 Gaussian Beam

Another test of the validly of the computational treatment is to verify it behaves as expected for a Gaussian beam profile. For instance a beam of amplitude varying as a Gaussian function:

$$f(x) = ae^{-\left[\frac{x - b}{c} \right]^2} \tag{3.14}$$

where a, b and c are constants. A Gaussian intensity distribution over the incoming wavefront should give in the image plane another Gaussian

---

[6]The constant a actually corresponds to $\frac{\text{radius of aperture}}{\text{focal length}}$.
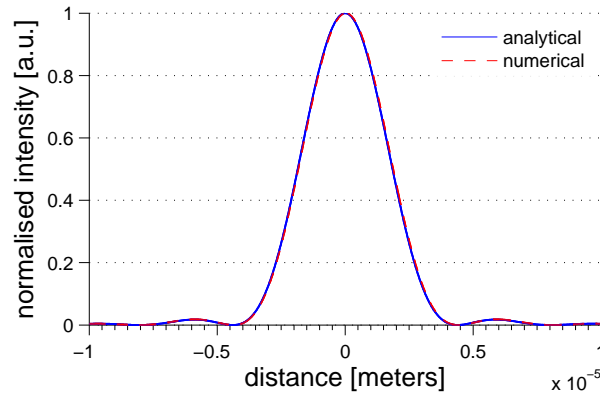
Figure 3.3: Predicted intensity distribution for a continuous beam from code accross x-axis of image plane, and plot of analytical solution.

intensity profile in the focal plane. Furthermore the Gaussian beam has the unique property that the cross-section remains Gaussian even away from the plane of best focus. So to test this a Gaussian profile was produced for the incoming computational wavefront using

$$f(x) = e^{-\left[\frac{x}{2.5 \times 10^{-2}}\right]^2} \tag{3.15}$$

(So $a = 1$, $b = 0$ and $c = 0.025$). Then a focal length of 45cm aperture diameter of 10cm and wavelength of 800nm were used in the calculation. This yielded a 3D intensity distribution as shown in Figure 3.4. The Figure shows surfaces of constant intensity, and is normalised to the maximum intensity. This is close to the focal plane and so one can see the intensity distribution does not vary much in z. On the other hand Figure 3.5 shows the surface of 92% intensity of electromagnetic field far on either side of the focus. The cone shape is indicative of the fact that the intensity distribution does remain Gaussian even away from focal plane.
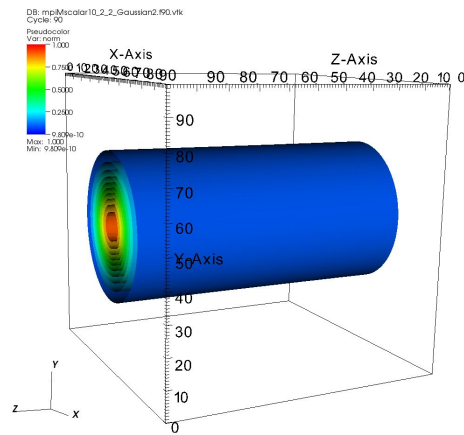
Figure 3.4: This is for a continuous Gaussian beam and shows the normalised intensity of the scalar electromagnetic field over real spacial dimensions. The steps along the axis are 2×10^{-8}m.
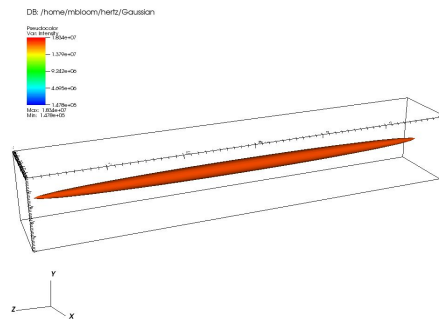

Figure 3.5: This is for a continuous Gaussian beam and shows the surface of 92% intensity for the scalar electromagnetic field over real spacial dimensions. The area shown is 60μm long in the z direction, with the plane of focus in its center. Each step along the axis is 4×10^{-7}m.

Looking at the intensity across a line crossing the center of the focal plane yielded an intensity profile shown in Figure 3.6. This profile was then fitted and found to be a Gaussian function:

$$f(x) = e^{-\left[\frac{x}{3.309 \times 10^{-6}}\right]^2} \tag{3.16}$$

A plot of this function is also shown in Figure 3.6 for comparison. This shows the code correctly models the behaviour of Gaussian beams.
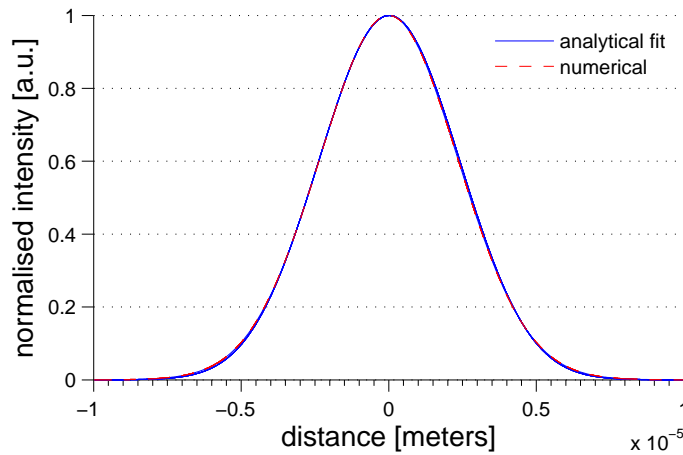

Figure 3.6: A line-out of the intensity through the focal plane due to a Gaussian beam. BLUE: The intensity predicted by the numerical code. RED: The Gaussian function shown in Equation 3.16.

3.3 Effects of Aberrations on Long Pulses

3.3.1 Astigmatisum

The nature of the aberration known as astigmatism is discussed in section 2.3. Figure 3.23 shows a the scalar electromagnetic field amplitude near to the focus cause by a continuous beam with an incident wavefront affected by this aberration.

3.3.2 Coma

Figures 3.7 and 3.8 show the field due to continuous beam effected by the aberration known as coma. The amount of coma in figure 3.8 is very large, much greater than would be experienced in most optical systems. Figure 3.7 shows a much smaller aberration by comparison, but still larger than one would expect in most modern optical systems. Note how the the most intense region moves to the left as the aberration is increased.
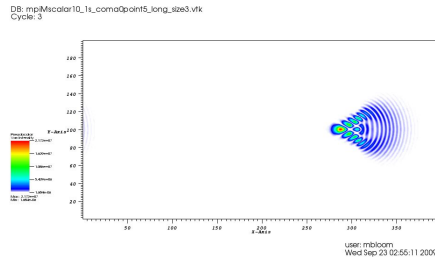
Figure 3.7: This is the magnitude of the scalar electromagnetic field in the image plane due to a continuous incident wave with an aberration of half a wavelengths of coma in the x direction. Each step on the axis represents 1μm in real space, with the unaberrated focus located at point (300,100).
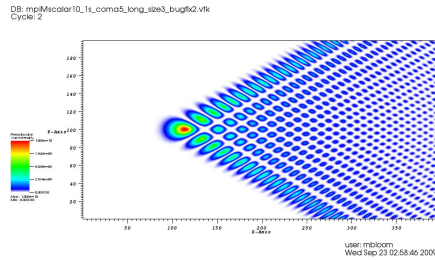
Figure 3.8: This is the magnitude of the scalar electromagnetic field in the image plane due to a continuous incident wave with an aberration of 5 full wavelengths of coma in the x direction. Each step on the axis represents 1μm in real space, with the unaberrated focus located at point (300,100).

3.4 Effects of Short Pulses

Now we move to looking at the effects of these aberrations on short pulsed beams. These results are interesting in so far as at the time of writing it would seem these effects have never been calculated before at least in this way.

3.4.1 Effect of Short Pulse Duration on a Uniform Wave Front (The Airy Pattern)

The 3d code was used to calculate the intensity distributions of the scalar electromagnetic filed about the center of focus for a 'flat' top beam profile with a pulse duration of only two full wavelengths. This is very short pulse duration but modern laser systems are now close to achieving pulses of only one wavelength duration. It is assumed that if short pulses make a significant change to the Airy ring pattern a pulse of this duration will make it most pronounced.

Figure 3.9 shows the result of this calculation (Figure 3.10 shows it from another view point)[7].

Figure 3.9: This is for a very short pulse of 2 wavelengths duration and shows the normalised intensity of the scalar electromagnetic field over real spacial dimensions. Note the line through the center represents the line-out of the same colour shown in Figure 3.12.

---

[7]The VisIt Visualisation Tool developed by the Lawrence Livermore National Laboratory was used to carry create these 3D images.

The images show surfaces of constant intensity and they are normalized to the central maxima's intensity. For comparison the same incident wavefront only with a continuous uniform intensity over time is calculated and shown in 3.11. In both figures the axis are of real space and the direction of propagation of the beam is in the positive Z direction. Note that qualitatively the short pulse has the 'lens' or 'rugby ball shape'. This is what is to be expected from the fact that only the parts of the source plane inside the light cone defined by the pulse envelope can interfere to create the outer Airy rings.
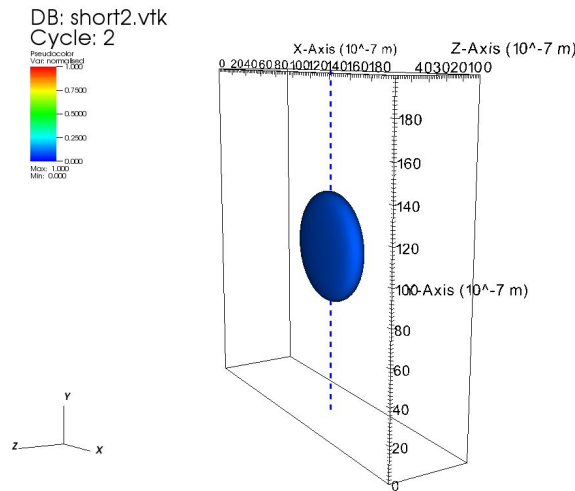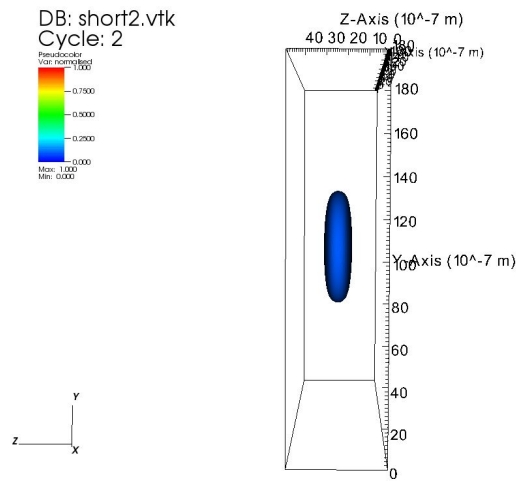

Figure 3.10: This is for a very short pulse of 2 wavelengths duration and shows the normalised intensity of the scalar electromagnetic field over real spacial dimensions. It essentially displays the same data as Figure 3.9 but from a different angle.

However for the purposes of a more quantitative analysis, Figure 3.12 shows line-outs of the diffraction patterns, (The position of the line-outs are shown in Figures 3.9 and 3.11). One can see from this that the Airy rings are reduced in the short pulsed case. The structure of the central peak is also slightly changed.

This is a significant result as in the case of for instance Laser Wakefield Accelerators [23] the power of even 1% of the diffraction pattern maximum intensity is enough to ionize the medium in which acceleration is to take place. Through tailoring diffraction pattern it is hoped that the way in which this happens can be controlled.

Figure 3.11: This is for a very long pulse (or a pulse of infinite duration) and shows the normalised intensity of the scalar electromagnetic field over real spacial dimensions. Note the line through the center represents the line-out of the same colour shown in Figure 3.12.
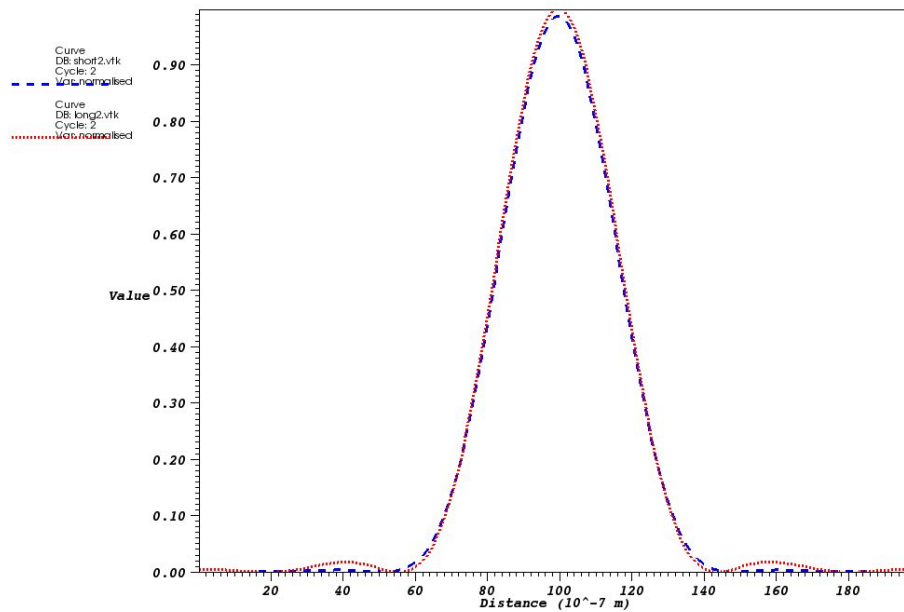
Figure 3.12: The BLUE line shows the relative intensity over the focal plane of a SHORT pulse. The RED shows the relative intensity over the focal plane of the LONG pulse.

Interestingly though, further analysis shows that the low intensity parts of the diffraction pattern are not uniform in time and actually have an opposite shape to the 'rugby ball' shown in Figure 3.9. If we look at the surface which represents 1% of the diffraction pattern maximum intensity shown in Figure 3.13. We see that the surface 'blooms out' at the ends of the pulse and forms a kind of 'saddle' shape. This is contrary to what one might expect. It represents the Airy pattern being present at the ends of the pulse but not in the center.
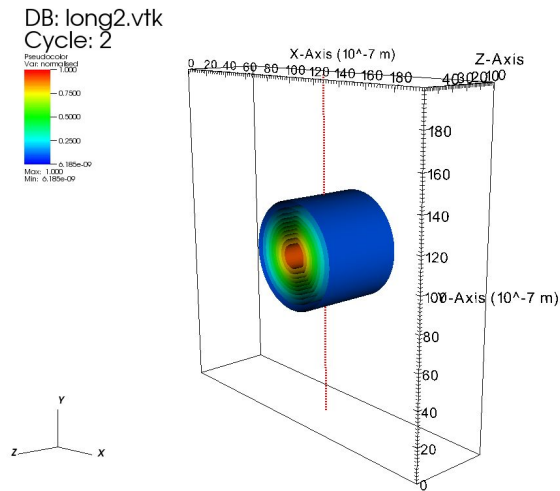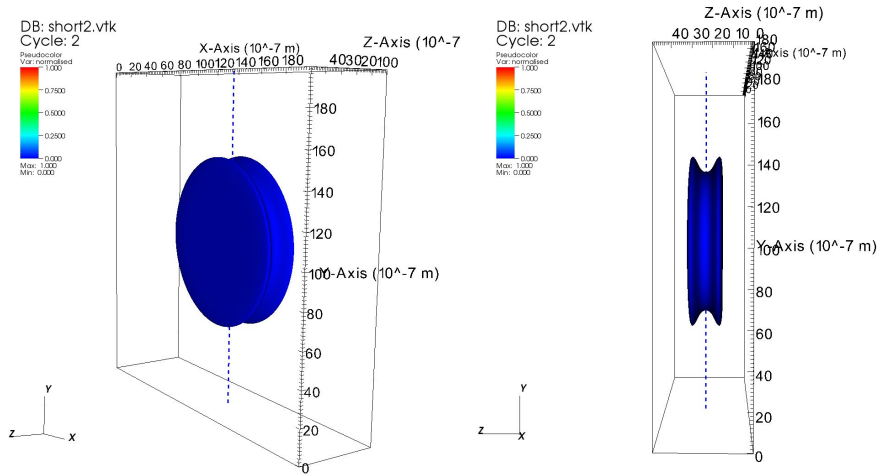

Figure 3.13: This is for a very short pulse of 2 wavelengths duration and shows the normalised intensity of the scalar electromagnetic field over real spacial dimensions. It essentially displays the same data as Figure 3.9 but the visible surface is of 1% of the maximum intensity.

This blooming effect seems to be limited to, in the case simulated here, the electromagnetic field less than 3% of the intensity maximum. Figures 3.14 to 3.19 show the surfaces. As you can see the effect seems to lessen until above 3% where the pulse shape returns to the familiar 'rugby ball'[8]. For the sake of comparison the corresponding surfaces for the continuous pulse are shown beside in Figures 3.15, 3.17 and 3.19. The surfaces shown in Figure 3.11 are reproduced on those plots only in black and white to avoid confusion. As one can see the surfaces of interest which bloom outwards correspond to the outer Airy rings[9].

---

[8]For completeness the surface visible in Figure 3.9 is 10% the maximum intensity.

[9]The surfaces for long and short pulses are normalised to the same value.

Figure 3.14: 1% surface. SHORT.

Figure 3.15: 1% surface. LONG.
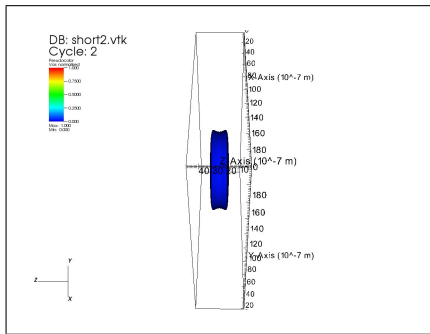
Figure 3.16: 2% surface. SHORT.
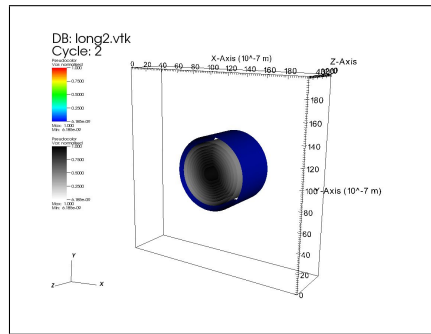
Figure 3.17: 2% surface. LONG.
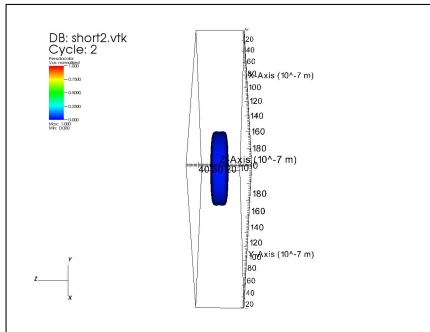
Figure 3.18: 3% surface. SHORT.
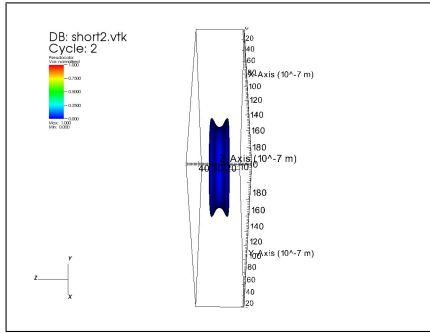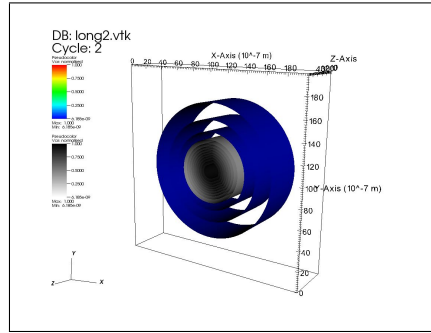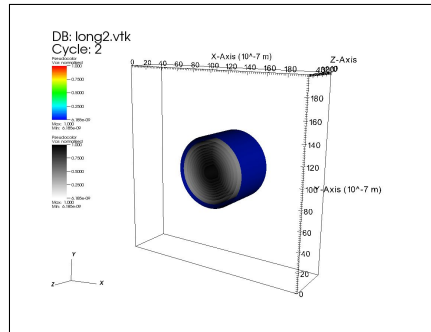

Figure 3.19: 3% surface. LONG.

3.4.2 Effect of Short Pulse Duration on Coma

Figure 3.20 and 3.21 show the intensity distribution across the focal plane due to a short pulse of 16 wavelengths. The conditions are the same as in long pulses (or for the purposes of this treatment continuous beams) in figures 3.7 and 3.8. One can see that the *coma tail* is smaller in the shorter pulse, for both the small and large amount of coma. See Chapter 5 for discussion. Figure 3.22 shows the distribution in 3D. The f-number is 4.5 in these.

Figure 3.20: BOTTOM: The magnitude of the scalar electromagnetic field in the image plane due to a short pulse of 16 wavelengths incident wave with an aberration of half a full wavelength of coma in the x direction. Each step on the axis represents 1μm in real space, with the unaberrated focus located at point (300,100). TOP: The equivalent for a continuous pulse (same as in Figure 3.7).

3.4.3 Effects of Short Pulse Duration on Astigmatism

Figure 3.24 shows the effect of Astigmatism on the time integrated intensity profile due to a pulse of 16 wavelengths. If you compare it to Figure 3.23 you can see the image is much the same only with the four low intensity trails (at North, South, East, and West) visibly lessened. This is in line with the other aberrations where the effect of short pulses appears to lessen

Figure 3.21: BOTTOM: The magnitude of the scalar electromagnetic field in the image plane due to a short pulse of 16 wavelenghs with an aberration of 5 full wavelengths of coma in the x direction. Each step on the axis represents 1μm in real space, with the unaberrated focus located at point (300,100). TOP: The equivalent for a continuous pulse (same as in Figure 3.8).

the spacial extent of the diffraction pattern. This is to be expected as the effect of a short pulse is to eliminate the constructive interference from far away points on the source plane of integration. These points are usually responsible for the diffraction pattern intensity far from the center of focus. Without them the diffraction pattern is lessened.
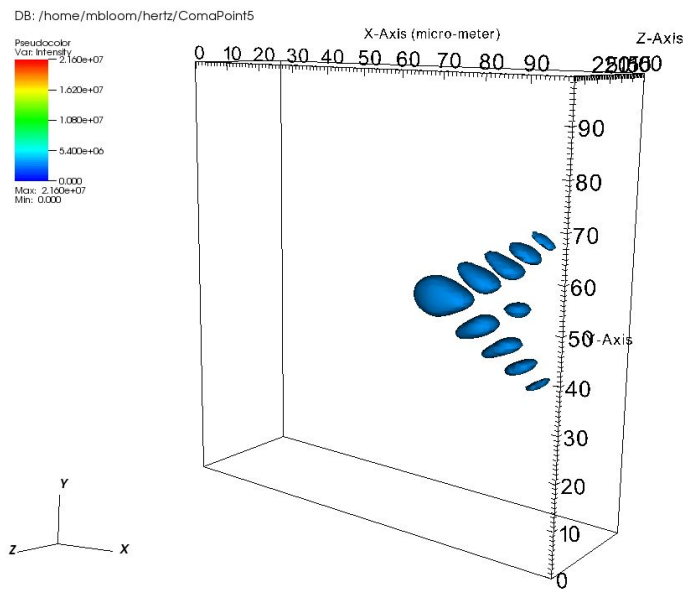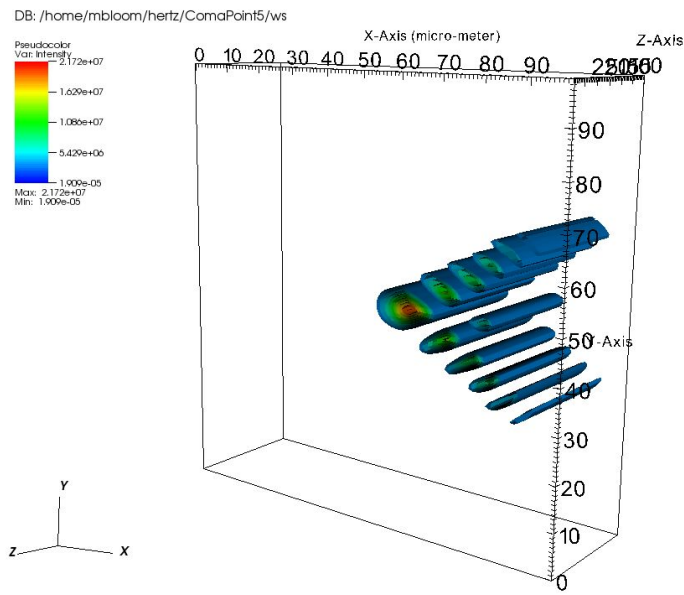
Figure 3.22: BOTTOM: 3D surface of constant intensity for the scalar electromagnetic field, near to the point of central focus, due to a short pulse of 16 wavelengths incident wave with an aberration of half a full wavelength of coma in the x direction. TOP: The equivalent for a continuous pulse.

For both figures the outer visible surface is of 15% of the maximum intensity. Each step on the axis represents 1μm in real space, with the unaberrated focus located in the center. The data sets are the same as in Figure 3.20.
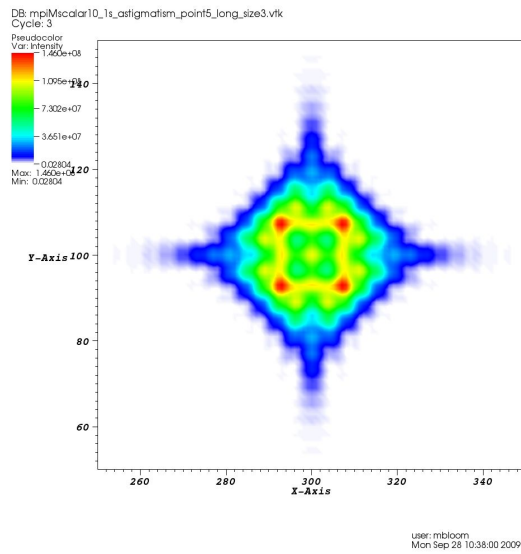
Figure 3.23: This is the magnitude of the scalar electromagnetic field in the image plane due to a continuous incident wave with an aberration of 0.5 wavelengths of 0° astigmatism in the x direction. Each step on the axis represents 1μm in real space, with the unaberated focus located at point (300,100). The wave length is 800nm, and the f number 9.
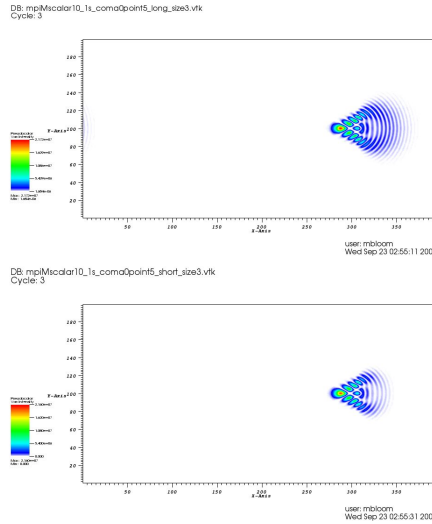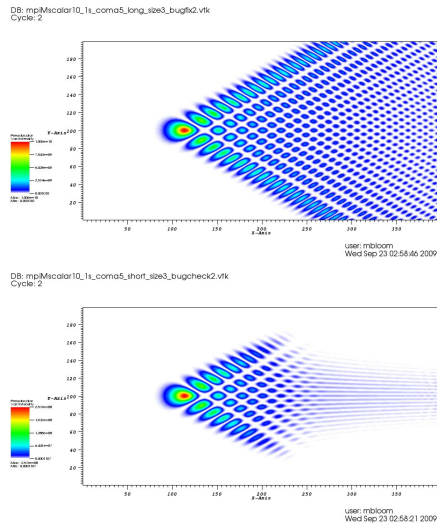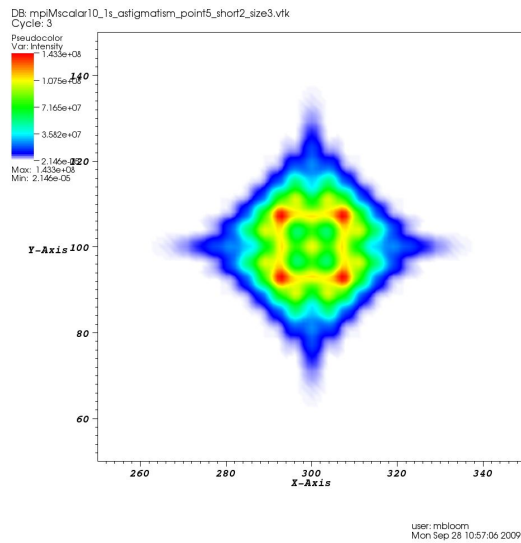

Figure 3.24: This is the magnitude of the scalar electromagnetic field in the image plane due to a incident pulse of 16 wavelengths with an aberration of 0.5 wavelengths of 0° astigmatism in the x direction. Each step on the axis represents 1μm in real space, with the unaberated focus located at point (300,100). The wave length is 800nm, and the f number 9.

43

4 Comparison of Numerical results with Experiment

4.1 Experiment
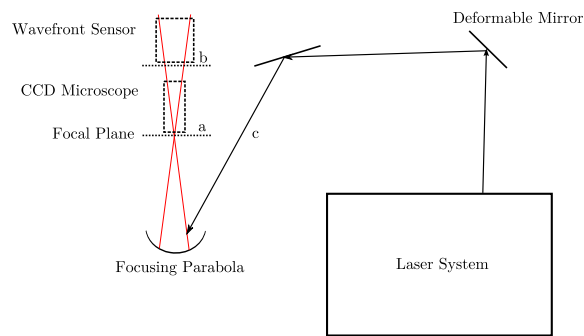
Figure 4.1: Schematic of the experimental layout. At point (a) a CCD camera with a microscope perspective can be added to the beam line to take the image shown in Figure 4.2. The aberrations to the wave front can be found through adding a wavefront sensor at point (b).

In [24] attempts were made to tailor the wavefront of a laser pulse used in a Laser-Wakefield Accelerator to control the x-rays produced. In doing so wave-fronts with coma were used and the intensity at the focus imaged. In the experiment an adaptive optics system was used. This consists of both a deformable mirror, before the focusing parabola, capable of introducing aberrations to the laser wavefront, and a wavefront sensor, capable of measuring the wave-front's intensity and phase. Through a feed back loop the system can attempt to introduce an aberration to the wave front and give a measurement in terms of the Zernike polynomial in Figure 2.6. The diffraction pattern caused by the focused beam was then measured by a CCD imaging device effectively at the focal plane. A schematic of the experimental layout is shown in Figure 4.1.

4.2 Analysis

Using the measured values for the experiment, provided by the authors of [24], it is possible to use the time integrating code (In appendix B.2) to create a computational estimation of the intensity that would been seen across the focal plane of the system. The time integrated image using all the experimental values from the experiment was produced and Figure 4.2 shows the experimental and computational images. For this experiment the f number of the system was 9. Corresponding to focusing surface of diameter 5cm and focal length of 45cm. The wavelength of the laser was 800nm and had a pulse length between 40fs and 45fs. This corresponds to pulse of approximately 16 wavelengths.

In Figure 4.2 one can see that the shape of the central peak is in strong correspondence between the two images. However there are two lobes in the experimental image which though present in the numerical image are far brighter. There also appears to be far more "coma ripples" in the experimental image, indicative of a larger degree of coma, and the fringes are closer together.

A possible explanation for the differences could include a non-linearity in the detector making the outer fringes more prominent in relation to the center. This is unlikely though due to the nature of the CCD system used and its tolerances.

The amplitude over the real wave front is not really a constant flat top as was assumed in our model and could go to explain some of the artifacts in this pattern. Further work includes using a measurement of a real lasers amplitude in simulation to gain a more realistic understating of this diffraction. However the fringes are unlikely due to the laser wavefronts shape in this case as it lacks the hard edges to create these aberrations. A possible source of the extra fringes could be an screening object such as a misaligned mirror clipping the edge of the beam. Great pains are taken by the experimentalists to avoid this but it can never be discounted. Even if a portion of the beam with 1% intensity is clipped, this can cause huge diffraction effects as this corresponds to 10% of the electric field being screened, which has large consequences when the fields go on to interfere. A similar problem is if there is a portion of, one of the many, mirrors involved not being of uniform reflectivity.

Additionally the pulse shape used in the simulation is arbitrary. Using a shape more accurately reflecting that in real laser beams could go towards solving some of the differences, and is a subject for further work.

Most of all it appears that there are extra aberrations present in the experimental image. This could well be the case. There could be a systematic error in recording the beams aberrations. For instance aberrations that are introduced and counterbalanced when the wavefront sensor is in the system but not present when the CCD is or other optical aberrations could be introduced out side the adaptive optics system and not recorded.

Further work is needed to explain these discrepancies not to mention one image is hardly representative however this at least shows that the code can be used to model real experimental systems.

experimental result

computational result
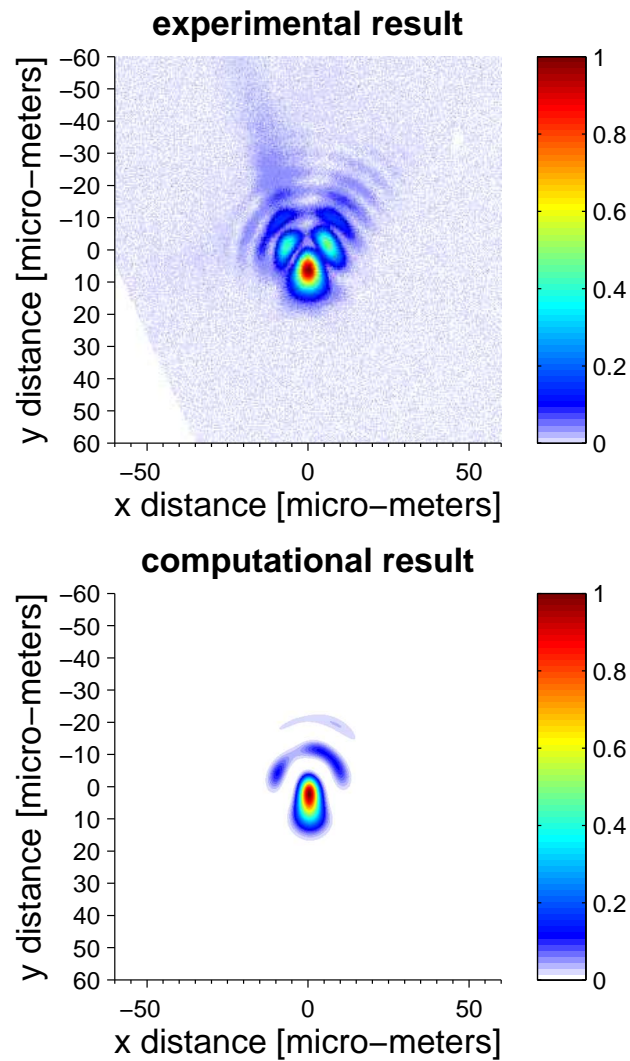
Figure 4.2: TOP: An image taken during experiment.
BELOW: A time integrated intensity profile calculated from the
aberrations reported for the experiment.
Both images have been normalised as a fraction of their peak
intensity.

5 Conclusion

To conclude, the computational model can calculate the 3D distribution of the scalar field in a reasonable time, reproduce analytical solutions and model real aberrations and intensity distributions.

Further work includes:

- Improving processing time of the code by changing the way it handles its memory allocations.

- Investigating the effects mentioned here in further detail using different focusing lengths and pulse lengths.

- Expanding the code to calculate the **E** and **B** from the scalar theory. Then verifying that the field distributions given by the code satisfy Maxwell's equations in all directions, through further numerical analysis.

- Basic integration for the phase variation over each cell in the source plane could be done to lower the number of points needed (The Runge-Kutta method).

- A new code utilising the Richards Wolf or Hertz Vector Diffraction Theory (HVDT) formalism, could be produced to observe the effects for low f-number systems and provide field vectors suitable for entry into PIC codes.

- Further work can be done on resolving the remaining differences between theory and experiment. Perhaps by fitting the aberrations found in experimental images.

5.1 Note on Beam Energy

There are two relevant things that categorise a diffraction pattern's intensity distribution. The magnitude of its central maxima and the distribution over

the rest of the pattern relative to that. It is of great interest to know what the effects of short pulses do to the central maxima's intensity in comparison to a long pulse [24]. Whether for instance there is more of the pulse's energy is located in the *central* maximum than in the *wings* for a shorter pulse

Unfortunately it is hard to draw clear conclusions about this as to do so it would be necessary to, in some way, compare the total energy in the long pulse, (which is essentially infinite but with constant power), to that in the short, which is of finite energy but varying power. Essentially the long pulse will always contain more energy that the short.
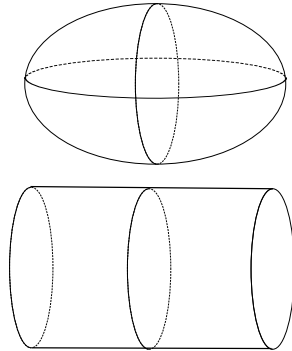
Figure 5.1: Schematic of an ideal truncated long pulse and a short pulse's field intensities distribution. ABOVE: Short. BELOW: Long.

Of course, over a finite time scale, the continuous pulse will have a certain diffraction pattern intensity distribution which will remain constant in time, whereas the short pulse will have a diffraction pattern intensity distribution which will evolve in time. For comparison the long pulse could always be truncated in time, but it will always have more electromagnetic flux than the short pulse. See figure 5.1, it is the parts missing from short pulse in comparison to the long that represent the difference in their diffraction pattern's intensities, but it is not clear how they effect the maximum intensity. From the results seen from the codes here it would appear that in the cases studied (for instance in section 3.4.1) the maximum intensity in the focal plane is not diminished, at least at the time when the pulse center is at the focal plane, but the outer rings' intensities are diminished.

However the matter of quantifying these effects, and comparing the magnitude of the pulse peaks, is a topic for future work. Here the relative intensity distribution was predominantly treated.

Bibliography

[1] Strickland D, Mourou G, Optics Communications, 56. P219. (1985)

[2] Chen P, Dawson JM, Huff RW, et al. Physical Review Letters. 54. P693. (1985)

[3] Mangles SPD, Murphy CD, Najmudin Z, et al. Nature. 431. p534. (2004)

[4] Donald Umstadter J. Phys. D: Appl. Phys. 36. 151-165. (2003)

[5] Chr. Huygens, *Traité de la Lumière* (Leyden, 1690);
English translation: *Treatise on Light* by S. P. Thompson, London, Macmillan & Co., 1912.

[6] G. Kirchoff, Berl. Ber. (1882), 641; Ann. d. Physik. (2), 18 (1883), 663; Ges. Abh. Nachtr., 22.

[7] M. Born & E. Wolf, 2002, "Principles of Optics", Seventh (Expanded) Ed. Cambridge University Press.

[8] J. D. Jackson, Classical Electrodynamics, Third Edition, John Wiley & Sons. (1999).

[9] Romallosa, KM; Bantang, J; Saloma, C; Three-dimensional light distribution near the focus of a tightly focused beam of few-cycle optical pulses; Physical Review A, 68 (3): Art. No. 033812 SEP 2003

[10] K. Schwarzschild, *Abh. Königl. Ges. Wis. Göttingen. Math-phys. KL.*, **4** (1905-1906), Nos. 1, 2, 3.

[11] L. Seidel, *Astr. Nachr.*, **43** (1856), No. 1027, 289, No. 1028, 305, No. 1029, 321.

[12] http://www.laser2000.co.uk, (September 2009).

[13] 3. E. Hecht, Optics, Addison-Wesley, Reading, Mass., (1987).

[14] B. B. Baker and E. T. Copson, The Mathematical Theory of Huygens Principle, 2nd ed. Clarendon, Oxford, UK, (1949).

[15] B. L and K. Duan, Nonparaxial propagation of vectorial Gaussian beams diffracted at a circular aperture, Opt. Lett 28, 24402442 (2003).

[16] K. Duan and B. L, Vectorial nonparaxial propagation equation of elliptical Gaussian beams in the presence of a rectangular aperture, J. Opt. Sec. Am. A 21, 16131620 (2004).

[17] B. Richards and E. Wolf, Electromagnetic diffraction in optical systems. II, Proc. R. Soc. London Ser. A 253, 358379 (1959).

[18] J. A. Stratton and L. J. Chu, Diffraction theory of electro-magnetic waves, Phys. Rev. 56, 99107 (1939).

[19] S. Guha, G. D. Gillen, Optics Express, 13, No. 5, 1424, (2005).

[20] Marathay, AS; McCalmont, JF; Vector diffraction theory for electromagnetic waves; Journal Of The Optical Society Of America A-Optics Image Science And Vision, 18 (10): 2585-2593 Oct (2001).

[21] S. A. Schelkunoff, Some equivalence theorems of electro-magnetics and their application to radiation problems, Bell Syst. Tech. J., January 15, 1936, pp. 99-112 (1936).

[22] S. A. Schelkunoff, Electromagnetic Waves, Van Nostrand, Princeton, N.J., pp. 331-373. (1943).

[23] A. G. R. Thomas, et al. Phys.Rev.Lett.98:095004, (2007).

[24] Mangles SPD, et al. arXiv:0909.3440v1 [physics.plam-ph] 18 Sep (2009).

A Derivation of integral theorem of Helmholtz and Kirchhoff

Here some steps in the derivation of the integral theroem of Helmholtz and Krchhoff will be expounded. This derivation is relevant to the discussion on page 10.

Equation (2.6) gives a singlarity at P so to avoid this let us define the integration region as in Figure A.1 where S' is a sphere about P with radus ε.
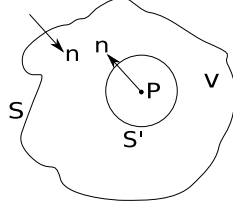
Figure A.1: integration regions

With the inclusion of these integration surfaces and equation (2.6), equation (2.5) can be writen

$$\left(\int\int_S + \int\int_{S'} \right) \left(U \frac{\partial}{\partial n} \left(\frac{e^{iks}}{s} \right) - \frac{e^{iks}}{s} \frac{\partial U}{\partial n} \right) dS = 0$$

$$\int\int_S \left(U \frac{\partial}{\partial n} \left(\frac{e^{iks}}{s} \right) - \frac{e^{iks}}{s} \frac{\partial U}{\partial n} \right) dS = -\int\int_{S'} \left(U \frac{\partial}{\partial n} \left(\frac{e^{iks}}{s} \right) - \frac{e^{iks}}{s} \frac{\partial U}{\partial n} \right) dS'$$

$$\int\int_S \left(U \frac{\partial}{\partial n} \left(\frac{e^{iks}}{s} \right) - \frac{e^{iks}}{s} \frac{\partial U}{\partial n} \right) dS = -\int\int_{S'} \left(U \frac{e^{iks}}{s} \left(ik - \frac{1}{s} \right) - \frac{e^{iks}}{s} \frac{\partial U}{\partial n} \right) dS'$$

$$\int\int_S \left(U \frac{\partial}{\partial n} \left(\frac{e^{iks}}{s} \right) - \frac{e^{iks}}{s} \frac{\partial U}{\partial n} \right) dS = -\int\int_{\omega} \left(U \frac{e^{ik\varepsilon}}{\varepsilon} \left(ik - \frac{1}{\varepsilon} \right) - \frac{e^{ik\varepsilon}}{\varepsilon} \frac{\partial U}{\partial s} \right) \varepsilon^2 d\omega$$

$$\int\int_S \left(U \frac{\partial}{\partial n} \left(\frac{e^{iks}}{s} \right) - \frac{e^{iks}}{s} \frac{\partial U}{\partial n} \right) dS = -\int\int_{\omega} \left(U e^{ik\varepsilon} \left(ik\varepsilon - 1 \right) - e^{ik\varepsilon} \varepsilon \frac{\partial U}{\partial s} \right) d\omega$$

Where it is noted over S', $s = \varepsilon$ and in the conversion to angular coordinates $dS' = \varepsilon^2 d\omega$. So as we take $\varepsilon \to 0$ all but the third term on the right hand side goes to zero. So evaluating the right hand side

$$\int\int_S \left(U \frac{\partial}{\partial n} \left(\frac{e^{iks}}{s} \right) - \frac{e^{iks}}{s} \frac{\partial U}{\partial n} \right) dS = \int\int_\omega U d\omega$$

$$\int\int_S \left(U \frac{\partial}{\partial n} \left(\frac{e^{iks}}{s} \right) - \frac{e^{iks}}{s} \frac{\partial U}{\partial n} \right) dS = 4\pi U(P)$$

which gives *integral theorem of Helmholtz and Kirchhoff* (2.7) (page 10).

B Transcrip of Source Codes

Two of the source codes produced and used as part of this project are provided below for interest and in the hope they might of some day be of use to a future student.

B.1 Three Dimensional Scalar Code

This code produces a 3D map of the scalar electromagnetic field about the center of focus.

```fortran
1  PROGRAM SCALAR
2      IMPLICIT NONE
3
4  include 'mpif.h'
5
6  !   Program mpiMscalar Version 10.1
7
8  !   Calculations use scalar diffraction theory over a section
        of a sphere.
9  !   There is no-inclination factor included.
10 !   Wave length = 800nm, Focal length = 45cm, Diameter = 5cm,
        So f number = 9
11 !   Aberrations are added by applying the first 15 Zernike
        Polynomials to the incoming wave front.
12 !   Finite Pulse length or continuous beam can be used.
        Amplitude function as(i,j) can be modified for very short
        pulses.
13 !   Source plane characterized by xs,ys,zs with phase delay
        delta compared to ideal spherical wavefront.
14
15 integer, parameter :: nxs=400, nys=400, nxi=200, nyi=100, nzi
        =50
16 real*8, dimension(nxs,nys) :: xs,ys,zs,delta,as
17 real*8, dimension(nxi,nyi,nzi) :: sr,si,gr,gi
```

```fortran
18    real*8 :: dxs,dys,dxi,dyi,dzi        ! step sizes in source and
         image planes
19    real*8 ::   xi,yi,zi                 ! current position in
         image plane
20    real*8 :: f,rmax, lambda            ! focal length and
         aperture radius
21    real*8 :: rmax2, rmax3, rmax4       ! powers of rmax for
         Zernike terms
22    real*8 :: pi, r, rs , phase
23    integer :: nproc, id , ierr         ! Used for MPI
24    integer :: i,j,ii,jj,kk,nchunk,i1,i2
25    real*8 :: xs0, ys0, xi0, yi0, zi0   ! starting positions in
         source and image
26    real*8 :: sumr, sumi, sum, amp, tau, t
27    real*8 :: coma, astig, sphab        ! primary aberrations
28    real*8 :: sintheta, costheta        ! angles for Zernike terms
29    ! Zernike Polynomials
30    real*8 :: z1, z2, z3, z4, z5, z6, z7, z8, z9, z10, z11, z12,
         z13, z14, z15
31    real*8 :: cz1, cz2, cz3, cz4, cz5, cz6, cz7, cz8, cz9, cz10,
         cz11, cz12, cz13, cz14, cz15
32    ! For the ease of computation
33    real*8 :: xs1, xs2, xs3, xs4, ys1, ys2, ys3, ys4
34
35
36    ! Initialise MPI
37       call MPI_Init(ierr)
38       call MPI_COMM_SIZE(MPI_COMM_WORLD, nproc, ierr)
39       call MPI_COMM_RANK(MPI_COMM_WORLD, id, ierr)
40       write (*,*) 'Process ', id, ' of ', nproc
41    ! Define Zernike constants
42     cz1 =     0.59
43     cz2 =     0.00
44     cz3 =     0.00
45     cz4 =     0.00
46     cz5 =    -0.01
47     cz6 =    -0.01
48     cz7 =    -0.18
49     cz8 =    -0.01
50     cz9 =    -0.01
51    cz10 =     0.02
52    cz11 =     0.01
```

```fortran
53    cz12 =     0.00
54    cz13 =     0.02
55    cz14 =     0.01
56    cz15 =    -0.01
57    ! Define other constants
58      pi = 4.0*atan2(1.0,1.0)
59      f = 45.0e-2               ! This is the focal length.
60      rmax = 5.0e-2             ! This the the aperture radius.
61      rmax2 = rmax*rmax
62      rmax3 = rmax2*rmax
63      rmax4 = rmax2*rmax2
64      lambda = 800.0e-9         ! This is the wavelength
65                                ! tau is half the total pulse
                                  !   duration, in periods in radians.
66      tau = 3.141592654*(16) ! The number in the brackets will
          now be the total wave lengths in the pulse.
67      dxs = 1.0e-3             ! Distance steps in x in the source
          plane.
68      dys = 1.0e-3             ! Distance steps in y in the source
          plane.
69      dxi = 0.2e-6             ! Distance steps in x in the image
          plane.
70      dyi = 0.2e-6             ! Distance steps in y in the image
          plane.
71      dzi = 0.2e-6             ! Distance steps in z in the image
          plane.
72      xs0 = -nxs*dxs/2.0
73      ys0 = -nys*dys/2.0
74      xi0 = -(nxi/2)*dxi
75      yi0 = -(nyi/2)*dyi
76      zi0 = -(nzi/2)*dzi
77    ! Define source properties
78      do i = 1, nxs
79        do j = 1, nys
80    ! This creates the spherical integration surface and gives
          each point a phase for corresponding to any aberrations.
81          xs(i,j) = xs0 + (i-1)*dxs
82          ys(i,j) = ys0 + (j-1)*dys
83          rs = xs(i,j)*xs(i,j) + ys(i,j)*ys(i,j)
84          zs(i,j) = f - sqrt(f*f - rs)
85          ! This 'if' decides the incoming wavefront intensity
              distribution in terms of x,y.
```

```fortran
86          if (rs .le. rmax2) then
87              as(i,j) = 1.0                    ! Include this line
                    for a Flat Top Beam Profile.
88  !           as(i,j) = exp(-4.0*rs/rmax2)   ! Iinclude this line
        for a Gaussian profile.
89          else
90              as(i,j) = 0.0
91          endif
92          !  Some checkpoint calculations
93          xs1 = xs(i,j)/rmax
94          xs2 = xs1*xs1
95          xs3 = xs1*xs2
96          xs4 = xs1*xs3
97          ys1 = ys(i,j)/rmax
98          ys2 = ys1*ys1
99          ys3 = ys1*ys2
100         ys4 = ys1*ys3
101         !   These are the Zernike normalisations.
102          z1 = 1
103
104          z2 = 2.0*xs1
105          z3 = 2.0*ys1
106
107          z4 = sqrt(3.0d0)*(2.0*xs2 + 2.0*ys2 - 1.0)
108          z5 = sqrt(6.0d0)*(xs2 - ys2)
109          z6 = sqrt(6.0d0)*(2.0*xs1*ys1)
110
111          z7 = sqrt(8.0d0)*(3.0*xs3 + 3.0*xs1*ys2 - 2.0*xs1)
112          z8 = sqrt(8.0d0)*(3.0*xs2*ys1 + ys3 - 2.0*ys1)
113          z9 = sqrt(8.0d0)*(xs3 - 3.0*xs1*ys2)
114         z10 = sqrt(8.0d0)*(3.0*xs2*ys1 - ys3)
115
116         z11 = sqrt(5.0d0)*(6.0*xs4 + 12.0*xs2*ys2 + 6.0*ys4 -
                6.0*xs2 - 6.0*ys2 + 1.0)
117         z12 = sqrt(10.0d0)*(4.0*xs4 - 3.0*xs2 + 3.0*ys2 - 4.0*
                ys4)
118         z13 = sqrt(10.0d0)*(8.0*xs3*ys1 + 8.0*xs1*ys3 - 6.0*xs1
                *ys1)
119         z14 = sqrt(10.0d0)*(xs4 - 6.0*xs2*ys2 + 4.0*ys4)
120         z15 = sqrt(10.0d0)*(xs3*ys1 - 4.0*xs1*ys3)
121
122         delta(i,j) = z1*cz1+z2*cz2+z3*cz3+z4*cz4+z5*cz5+z6*cz6+
```

```fortran
                      z7*cz7+z8*cz8+z9*cz9+z10*cz10+z11*cz11+z12*cz12+z13
                      *cz13+z14*cz14+z15*cz15
123  !        write(*,*) delta(i,j)
124  !        delta(i,j) = 0.0
125         enddo
126       enddo
127  !
128  ! Split the x loop in Image space among the MPI processes
129     nchunk = nxi/nproc
130     i1 = 1 + id*nchunk
131     i2 = i1 + nchunk -1
132  ! Last process gets tail end of loop
133     if(id .eq. nproc-1) i2 = nxi
134     write(*,*)'Process ',id,' Iterations ',i1,i2
135
136     do ii = i1, i2
137       write(*,*)'X iteration ', ii
138       do jj = 1, nyi
139         do kk = 1, nzi
140           xi = xi0 + (ii-1)*dxi
141           yi = yi0 + (jj-1)*dyi
142           zi = f + zi0 + (kk-1)*dzi
143  !  prepare for the numerical integration over source plane
144           sumr = 0.0
145           sumi = 0.0
146           do i = 1, nxs
147             do j = 1, nys
148               r = sqrt((xs(i,j)-xi)*(xs(i,j)-xi) + (ys(i,j)-yi)
                      *(ys(i,j)-yi) &
149               +    (zs(i,j)-zi)*(zs(i,j)-zi) )
150  ! THIS IS WHERE COMA AND OTHER ABERRATIONS ARE ADDED TO THE
         CALCULATION
151               phase = 2.0*pi*( (r-f)/lambda + delta(i,j) )
152  ! we adjust the amplitude in the source plane due to the time
          delay
153  ! implied by the phase delay .  The polynomial is a simple
         envelope fn
154               t = abs(phase / tau)
155  ! Include the following loop to limit the pulse length.
156               if (t .ge. 1.0) then
157                 amp = 0.0
158               else
```

```fortran
159                    amp = as(i,j)*(t*t*t*t - 2.0*t*t + 1.0)
160                endif
161 !                amp = as(i,j)    ! remove/include this line if
         using finite pulse length
162 !                Inclination factor can be included here.
163                sumi = sumi + amp*cos(phase)/r    ! *(sqrt((xs(i,j
                     )-xi)*(xs(i,j)-xi) + (ys(i,j)-yi)*(ys(i,j)-yi
                     )))/(r*r)
164                sumr = sumr + amp*sin(phase)/r    ! *(sqrt((xs(i,j
                     )-xi)*(xs(i,j)-xi) + (ys(i,j)-yi)*(ys(i,j)-yi
                     )))/(r*r)
165             enddo
166            enddo
167            sr(ii,jj,kk)=sumr
168            si(ii,jj,kk)=sumi
169          enddo
170        enddo
171      enddo
172 ! get all the chunks together on processor zero
173      call MPI_REDUCE(sr,gr,nxi*nyi*nzi,MPI_REAL8,MPI_SUM,0,
            MPI_COMM_WORLD,ierr)
174      call MPI_REDUCE(si,gi,nxi*nyi*nzi,MPI_REAL8,MPI_SUM,0,
            MPI_COMM_WORLD,ierr)
175      call MPI_FINALIZE(ierr)
176
177      if (id .eq. 0) then
178
179 ! Makes the VTK file.
180      call VTK(gr, gi, nxi, nyi, nzi)
181
182      endif
183
184  END PROGRAM SCALAR
185
186 ! This Subroutine writes the results of the calculation to a
        .vtk file format.
187 ! for use with the VisIt Visualisation Tool developed by the
        Lawrence Livermore National Laboratory
188
189      subroutine VTK(data,datai,nx,ny,nz)
190      integer :: nx, ny, nz
191      real*8 :: data(nx,ny,nz), datai(nx,ny,nz)
```

```fortran
192      real*8 :: intensity, phase
193      integer :: i, j, k
194
195      do i = 1, nx
196        do j = 1, ny
197          do k = 1, nz
198            intensity = data(i,j,k)*data(i,j,k) + datai(i,j,k)*
                   datai(i,j,k)
199            phase = atan2(data(i,j,k), datai(i,j,k))
200            data(i,j,k) = intensity
201            datai(i,j,k) = phase
202          enddo
203        enddo
204      enddo
205
206      open(unit=10,file='scalar.vtk',form='formatted', access='
             stream')
207      write(10,'("#_vtk_DataFile_Version_2.0")')
208      write(10,'("Diffraction_code")')
209      write(10,'("ASCII")')
210      write(10,'("DATASET_STRUCTURED_POINTS")')
211      write(10,'("DIMENSIONS_",3i5)') nx, ny, nz
212      write(10,'("SPACING_1_1_1")')
213      write(10,'("ORIGIN_0_0_0")')
214      write(10,'("POINT_DATA_",i9)') nx*ny*nz
215      write(10,'("SCALARS_Intensity_float_1")')
216      write(10,'("LOOKUP_TABLE_default")')
217      write(10,'(1p6e11.4)') data
218 !  The second scalar dataset
219      write(10,'("SCALARS_Phase_float_1")')
220      write(10,'("LOOKUP_TABLE_default")')
221      write(10,'(1p6e11.4)') datai
222
223      close(10)
224      end subroutine VTK
```

B.2 Time Integrated Scalar Code

This code produces a 2D plot of the time integrated intensity of the scalar electromagnetic field on the image plane (This can be changed through the variable zi).

```fortran
1  PROGRAM SCALAR
2      IMPLICIT NONE
3
4  include 'mpif.h'
5
6  !   Program mpiMscalar_TIME  Version 8.71
7
8  !   This program produces a 'time integrated' image of the
       focal plane.
9  !   This should give a good indication of what imaging device
       would record.
10 !   This program   creates a number of  images  (n='tnt') in
       the focal plane separated by a time delay.
11 !   The images are then added to give an time integrated image
12 !   and so gives a   relative intensity distribution which
       might be observed.
13 !   4 Text files will be produced with the REAL, IMAGINARY,
       INTENSITY, PHASE images.
14 !   These are space deliminated.
15 !   A VTK file is produced with the time separated images. (
       Time is varied along the Z axis)
16
17 !   Calculations use scalar diffraction theory over a section
       of a sphere.
18 !   There is no-inclination factor included.
19 !   Wave length = 800nm, Focal length = 45cm, Diameter = 5cm,
       So f number = 9
20 !   Aberrations are added by applying the first 15 Zernike
       Polynomials to the incoming wave front.
21 !   Finite Pulse length or continuous beam can be used.
22 !   Amplitude function as(i,j) can be modified for very short
       pulses.
23 !   Source plane characterised by xs,ys,zs with phase delay
       delta compared to ideal spherical wavefront.
24
25 integer, parameter :: nxs=400, nys=400, nxi=100, nyi=100, tnt
```

```fortran
              =30 ! Number of steps in x, y, and time.
26    real*8, dimension(nxs,nys) :: xs,ys,zs,delta,as
27    real*8, dimension(nxi,nyi,tnt) :: sr,si,gr,gi
28    real*8 :: dxs,dys,dxi,dyi,dzi        ! step sizes in source and
           image planes
29    real*8 ::  xi,yi,zi                  ! current position in
           image plane
30    real*8 ::  f,rmax, lambda           ! focal length and
           aperture radius
31    real*8 :: rmax2, rmax3, rmax4        ! powers of rmax for
           Zernike terms
32    real*8 :: pi, r, rs, phase
33    integer :: nproc, id, ierr          ! Used for MPI
34    integer :: i,j,ii,jj,kk,nchunk,i1,i2,tt
35    real*8 :: xs0, ys0, xi0, yi0, zi0  ! starting positions in
           source and image
36    real*8 :: sumr, sumi, sum, amp, tau, t
37    real*8 :: coma, astig, sphab        ! primary aberrations
38    real*8 :: sintheta, costheta        ! angles for Zernike terms
39    ! Zernike Polynomials
40    real*8 :: z1, z2, z3, z4, z5, z6, z7, z8, z9, z10, z11, z12,
           z13, z14, z15
41    real*8 :: cz1, cz2, cz3, cz4, cz5, cz6, cz7, cz8, cz9, cz10,
           cz11, cz12, cz13, cz14, cz15
42    ! For the ease of computation
43    real*8 :: xs1, xs2, xs3, xs4, ys1, ys2, ys3, ys4
44    character(len=255) :: fx, fy        ! Strings for a formatting
           work around.
45    real*8, dimension(nxi,nyi,tnt) :: INTintensity, INTphase
46
47    ! Initialise MPI
48      call MPI_Init(ierr)
49      call MPI_COMM_SIZE(MPI_COMM_WORLD, nproc, ierr)
50      call MPI_COMM_RANK(MPI_COMM_WORLD, id, ierr)
51      write (*,*) 'Process ', id, ' of ', nproc
52    ! Define Zernike constants
53      cz1 =    0.59
54      cz2 =    0.00
55      cz3 =    0.00
56      cz4 =    0.00
57      cz5 =   -0.01
58      cz6 =   -0.01
```

```fortran
 59    cz7 =    -0.18
 60    cz8 =    -0.01
 61    cz9 =    -0.01
 62   cz10 =     0.02
 63   cz11 =     0.01
 64   cz12 =     0.00
 65   cz13 =     0.02
 66   cz14 =     0.01
 67   cz15 =    -0.01
 68  ! Define other constants
 69     pi = 4.0*atan2(1.0,1.0)
 70     f = 45.0e-2               ! This is the focal length.
 71     rmax = 5.0e-2             ! This the the aperture radius.
 72     rmax2 = rmax*rmax
 73     rmax3 = rmax2*rmax
 74     rmax4 = rmax2*rmax2
 75     lambda = 800.0e-9         ! This is the wavelength
 76                              ! tau is half the total pulse
                                   duration, in periods in radians.
 77     tau = 3.141592654*(16) ! The number in the brackets will
           now be the total wave lengths in the pulse.
 78     dxs = 1.0e-3             ! Distance steps in x in the source
           plane.
 79     dys = 1.0e-3             ! Distance steps in y in the source
           plane.
 80     dxi = 0.2e-6             ! Distance steps in x in the image
           plane.
 81     dyi = 0.2e-6             ! Distance steps in y in the image
           plane.
 82     dzi = 0.2e-6             ! Distance steps in z in the image
           plane.
 83     xs0 = -nxs*dxs/2.0
 84     ys0 = -nys*dys/2.0
 85     xi0 = -(nxi/2)*dxi
 86     yi0 = -(nyi/2)*dyi
 87     zi = f                   ! This sets where the time
           integrated image is located (here it is the focal plain
           )
 88  ! Define source properties
 89     do i = 1, nxs
 90       do j = 1, nys
 91  ! This creates the spherical integration surface and gives
```

```fortran
            each point a phase corresponding to any aberrations.
92             xs(i,j) = xs0 + (i-1)*dxs
93             ys(i,j) = ys0 + (j-1)*dys
94             rs = xs(i,j)*xs(i,j) + ys(i,j)*ys(i,j)
95             zs(i,j) = f - sqrt(f*f - rs)
96             ! This 'if' decides the incoming wavefront intensity
                     distribution in terms of x,y.
97             if (rs .le. rmax2) then
98                 as(i,j) = 1.0                    ! Include this line
                        for a Flat Top Beam Profile.
99  !              as(i,j) = exp(-4.0*rs/rmax2)   ! Include this line
         for a Gaussian profile.
100            else
101                as(i,j) = 0.0
102            endif
103            !  Some checkpoint calculations
104            xs1 = xs(i,j)/rmax
105            xs2 = xs1*xs1
106            xs3 = xs1*xs2
107            xs4 = xs1*xs3
108            ys1 = ys(i,j)/rmax
109            ys2 = ys1*ys1
110            ys3 = ys1*ys2
111            ys4 = ys1*ys3
112            !   These are the Zernike normalisations.
113             z1 = 1
114
115             z2 = 2.0*xs1
116             z3 = 2.0*ys1
117
118             z4 = sqrt(3.0d0)*(2.0*xs2 + 2.0*ys2 - 1.0)
119             z5 = sqrt(6.0d0)*(xs2 - ys2)
120             z6 = sqrt(6.0d0)*(2.0*xs1*ys1)
121
122             z7 = sqrt(8.0d0)*(3.0*xs3 + 3.0*xs1*ys2 - 2.0*xs1)
123             z8 = sqrt(8.0d0)*(3.0*xs2*ys1 + ys3 - 2.0*ys1)
124             z9 = sqrt(8.0d0)*(xs3 - 3.0*xs1*ys2)
125            z10 = sqrt(8.0d0)*(3.0*xs2*ys1 - ys3)
126
127            z11 = sqrt(5.0d0)*(6.0*xs4 + 12.0*xs2*ys2 + 6.0*ys4 -
                    6.0*xs2 - 6.0*ys2 + 1.0)
128            z12 = sqrt(10.0d0)*(4.0*xs4 - 3.0*xs2 + 3.0*ys2 - 4.0*
```

```fortran
                ys4)
129         z13 = sqrt(10.0d0)*(8.0*xs3*ys1 + 8.0*xs1*ys3 − 6.0*xs1
                *ys1)
130         z14 = sqrt(10.0d0)*(xs4 − 6.0*xs2*ys2 + 4.0*ys4)
131         z15 = sqrt(10.0d0)*(xs3*ys1 − 4.0*xs1*ys3)
132
133         delta(i,j) = z1*cz1+z2*cz2+z3*cz3+z4*cz4+z5*cz5+z6*cz6+
                z7*cz7+z8*cz8+z9*cz9+z10*cz10+z11*cz11+z12*cz12+z13
                *cz13+z14*cz14+z15*cz15
134 !       write(*,*) delta(i,j)
135 !       delta(i,j) = 0.0
136     enddo
137   enddo
138
139 ! Split the x loop in Image space among the MPI processes
140   nchunk = nxi/nproc
141   i1 = 1 + id*nchunk
142   i2 = i1 + nchunk −1
143 ! Last process gets tail end of loop
144   if(id .eq. nproc−1) i2 = nxi
145   write(*,*)'Process ',id,' Iterations ',i1,i2
146
147 do tt = 1, tnt
148   do ii = i1 , i2
149     write(*,*)'X iteration ', ii
150     do jj = 1, nyi
151
152         xi = xi0 + (ii −1)*dxi
153         yi = yi0 + (jj −1)*dyi
154
155 !       zi = f                    ! This line has been taken out of
        the loop and put at the top for faster processing.
156 !  prepare for the numerical integration over source plane
157         sumr = 0.0
158         sumi = 0.0
159         do i = 1, nxs
160           do j = 1, nys
161             r = sqrt((xs(i,j)−xi)*(xs(i,j)−xi) + (ys(i,j)−yi)
                *(ys(i,j)−yi) &
162             +    (zs(i,j)−zi)*(zs(i,j)−zi) )
163             phase = 2.0*pi*( (r−f)/lambda + delta(i,j) )
164 ! we adjust the amplitude in the source plane due to the time
```

```
          delay
165  ! implied by the phase delay. The polynomial is a simple
          envelope fn
166              t = (phase / tau) - 1.50 +float(tt-1)*3.0/float(
                  tnt-1)
167  ! write(*,*) "time loop", tt, t          ! Include this line
          to have a print out of the t function for trouble
          shooting.
168  ! Include the following loop to limit the pulse length.
169              if (abs(t) .ge. 1.0) then
170                  amp = 0.0
171              else
172                  amp = as(i,j)*(t*t*t*t - 2.0*t*t + 1.0)
173              endif
174  !          amp = as(i,j)    ! remove/include this line if
          using finite pulse length
175  !          Inclination factor removed here.
176              sumi = sumi + amp*cos(phase)/r  !*(sqrt((xs(i,j)-
                  xi)*(xs(i,j)-xi) + (ys(i,j)-yi)*(ys(i,j)-yi))
                  )/(r*r)
177              sumr = sumr + amp*sin(phase)/r  !*(sqrt((xs(i,j)-
                  xi)*(xs(i,j)-xi) + (ys(i,j)-yi)*(ys(i,j)-yi))
                  )/(r*r)
178          enddo
179        enddo
180        sr(ii,jj,tt)=sumr
181        si(ii,jj,tt)=sumi
182      enddo
183    enddo
184  enddo
185  ! get all the chunks together on processor zero
186  call MPI_REDUCE(sr,gr,nxi*nyi*tnt,MPI_REAL8,MPI_SUM,0,
          MPI_COMM_WORLD,ierr)
187  call MPI_REDUCE(si,gi,nxi*nyi*tnt,MPI_REAL8,MPI_SUM,0,
          MPI_COMM_WORLD,ierr)
188  call MPI_FINALIZE(ierr)
189
190  if (id .eq. 0) then
191  ! Makes the VTK file.
192  call VTK(gr, gi, nxi, nyi, tnt)
193
194  !   This is the time integration
```

```fortran
195        do ii= 1,nxi
196           do jj=1,nyi
197              sumr=0.0
198              sumi=0.0
199              do tt= 1, tnt
200                 sumr=sumr+gr(ii,jj,tt)
201                 sumi=sumi+gi(ii,jj,tt)
202              enddo
203              gr(ii,jj,1)=sumr      ! Here the first row of gr and
                                          gi is reused to store the images.
204              gi(ii,jj,1)=sumi
205           enddo
206        enddo
207  ! This should write out tables for the time integrated image.
208  ! Real and imaginary values:
209    open(unit=30,file='Rintergrated.txt',form='formatted',
            access='append')
210    open(unit=40,file='Iintergrated.txt',form='formatted',
            access='append')
211  ! The over all intensity: R^2 + I^2 (the 'S' stands for sum)
212    open(unit=50,file='Sintergrated.txt',form='formatted',
            access='append')
213  ! The phase: atan2(R, I)
214    open(unit=60,file='Pintergrated.txt',form='formatted',
            access='append')
215  ! This is to create a string to use as the format information
            for the write command
216  ! So 'fy' is the format for writing nyi columns.
217    write(fy,'("(",I3,"e11.4)")')nyi
218    write(fx,'("(",I3,"e11.4)")')nxi
219  ! Writes file 'Rintergrated.txt'.
220    do ii=1, nxi
221       write(30,fy)(gr(ii,jj,1),jj=1,nyi)
222    enddo
223  ! Writes file 'Iintergrated.txt'.
224    do ii=1, nxi
225       write(40,fy)(gi(ii,jj,1),jj=1,nyi)
226    enddo
227  ! Calculates the Intensity and Phase values.
228    do ii = 1, nxi
229       do jj = 1, nyi
230             INTintensity(ii,jj,1) = gr(ii,jj,1)*gr(ii,jj,1) + gi(
```

```fortran
                    ii ,jj ,1)*gi(ii ,jj ,1)
231             INTphase = atan2(gr(ii ,jj ,1) , gi(ii ,jj ,1))
232         enddo
233     enddo
234 ! Writes file 'Sintergrated.txt'.
235   do ii =1, nxi
236       write(50,fy)(INTintensity(ii ,jj ,1),jj=1,nyi)
237   enddo
238 ! Writes file 'Pintergrated.txt'.
239   do ii =1, nxi
240       write(60,fy)(INTphase(ii ,jj ,1),jj=1,nyi)
241   enddo
242
243 endif
244
245  END PROGRAM SCALAR
246
247 ! This Subroutine writes the results of the calculation to a
          .vtk file format.
248 ! for use with the VisIt Visualisation Tool developed by the
          Lawrence Livermore National Laboratory
249
250   subroutine VTK(data, datai ,nx,ny,nz)
251   integer :: nx, ny, nz
252   real*8 :: data(nx,ny,nz), datai(nx,ny,nz)
253   real*8 :: intensity , phase
254   integer :: i, j, k
255   do i = 1, nx
256     do j = 1, ny
257       do k = 1, nz
258           intensity = data(i,j,k)*data(i,j,k) + datai(i,j,k)*
                  datai(i,j,k)
259           phase = atan2(data(i,j,k), datai(i,j,k))
260           data(i,j,k) = intensity
261           datai(i,j,k) = phase
262       enddo
263     enddo
264   enddo
265
266   open(unit=10,file='scalar.vtk',form='formatted', access='
          stream')
267   write(10,'("#_vtk_DataFile_Version_2.0")')
```

```fortran
268    write(10,'("Diffraction_code")')
269    write(10,'("ASCII")')
270    write(10,'("DATASET_STRUCTURED_POINTS")')
271    write(10,'("DIMENSIONS_",3i5)') nx, ny, nz
272    write(10,'("SPACING_1_1_1")')
273    write(10,'("ORIGIN_0_0_0")')
274    write(10,'("POINT_DATA_",i9)') nx*ny*nz
275    write(10,'("SCALARS_Intensity_float_1")')
276    write(10,'("LOOKUP_TABLE_default")')
277    write(10,'(1p6e11.4)') data
278  ! The second scalar dataset
279    write(10,'("SCALARS_Phase_float_1")')
280    write(10,'("LOOKUP_TABLE_default")')
281    write(10,'(1p6e11.4)') datai
282
283    close(10)
284    end subroutine VTK
```